10. Yasuda S, Townsend D, Michele DE, et al. Dystrophic heart failure blocked by membrane sealant poloxamer. Nature 2005;436:1025-9.
11. Yoshimura M, Sakamoto M, Ikemoto M, et al. AAV vector-mediated microdystrophin expression in a relatively small percentage of mdx myofibers improved the mdx phenotype. Mol Ther 2004;10:821-8.
12. Dezawa M, Ishikawa H, Itokazu Y, et al. Bone marrow stromal cells generate muscle cells and repair muscle degeneration. Science 2005;309:314-7.
13. Dell'Agnola C, Wang Z, Storb R, et al. Hematopoietic stem cell transplantation does not restore dystrophin expression in Duchenne muscular dystrophy dogs. Blood 2004;104:4311-8.
14. Wilton SD, Honeyman K, Fletcher S, et al. Snapback SSCP analysis: engineered conformation changes for the rapid typing of known mutations. Hum Mutat 1998;11:252-8.
15. Valentine BA, Cooper BJ, de Lahunta A, et al. Canine X-linked muscular dystrophy. An animal model of Duchenne muscular dystrophy: clinical studies. J Neurol Sci 1988;88:69-81.
16. Kornegay JN, Bogan DJ, Bogan JR, et al. Contraction force generated by tarsal joint flexion and extension in dogs with golden retriever muscular dystrophy. J Neurol Sci 1999;166:115-21.
17. Bartlett RJ, Winand NJ, Secore SL, et al. Mutation segregation and rapid carrier detection of X-linked muscular dystrophy in dogs. Am J Vet Res 1996;57:650-4.
18. Valentine BA, Cooper BJ. Canine X-linked muscular dystrophy: selective involvement of muscles in neonatal dogs. Neuromuscul Disord 1991;1:31-8.
19. Nguyen F, Cherel Y, Guigand L, et al. Muscle lesions associated with dystrophin deficiency in neonatal golden retriever puppies. J Comp Pathol 2002;126:100-8.
20. Seksel K. Puppy socialization classes. Vet Clin North Am Small Anim Pract 1997;27:465-77.
21. Valentine BA, Cooper BJ, Cummings JF, et al. Canine X-linked muscular dystrophy: morphologic lesions. J Neurol Sci 1990;97:1-23.
22. Jaffe KM, McDonald CM, Ingman E, et al. Symptoms of upper gastrointestinal dysfunction in Duchenne muscular dystrophy: case-control study. Arch Phys Med Rehabil 1990;71:742-4.
23. Willig TN, Paulus J, Lacau Saint Guily J, et al. Swallowing problems in neuromuscular disorders. Arch Phys Med Rehabil 1994;75:1175-81.

American Journal of Pathology, Vol. 166, No. 6, June 2005

Musculoskeletal Pathology

Participation of Bone Marrow-Derived Cells in Fibrotic Changes in Denervated Skeletal Muscle

Yasushi Mochizuki,*† Koichi Ojima,* Akiyoshi Uezumi,* Satoru Masuda,* Kotaro Yoshimura,† and Shin'ichi Takeda*

From the Department of Molecular Therapy, National Institute of Neuroscience, National Center of Neurology and Psychiatry, Ogawa-higashi-cho, Kodaira, Tokyo; and the Department of Plastic and Reconstructive Surgery,† Graduate School of Medicine, The University of Tokyo, Hongo, Bunkyo-ku, Tokyo, Japan*

In denervated skeletal muscle, mononuclear interstitial cells accumulate in the perisynaptic regions before fibrotic change occurs. These cells are currently considered to be fibroblasts that originate from muscle tissue. However, when we denervated hind limbs of GFP-bone marrow chimeric mice by excising the sciatic nerve unilaterally, many bone marrow-derived cells (BM-DCs) infiltrated the interstitial spaces and accumulated in the perisynaptic regions, peaking 14 days after denervation. They accounted for nearly one-half of the increase in mononuclear interstitial cells. Although BM-DCs did not incorporate into satellite cells, immunohistochemical and FACS analyses revealed that BM-DCs were both CD45 and CD11b positive, indicating that they were of macrophage/monocyte lineage. BrdU staining showed inactive proliferation of BM-DCs. Reverse transcriptase-polymerase chain reaction of mononuclear cells isolated by FACS revealed that BM-DCs did not express type I collagen or tenascin-C; however, they did express transforming growth factor-β1, suggesting that they regulate the fibrotic process. In contrast, muscle tissue-derived interstitial cells expressed type I collagen and tenascin-C, suggesting that these populations were the final effectors of fibrosis. These findings identify elementary targets that may regulate the migration, homing, differentiation, and function of BM-DCs, leading to amelioration of the excessive fibrosis of denervated skeletal muscle. *(Am J Pathol 2005, 166:1721–1732)*

Fibrotic change is often observed after subacute or chronic inflammation, and severe fibrosis of a vital organ such as the lung, liver, or kidney is sometimes fatal. Denervated skeletal muscle tissue also exhibits persistent fibrotic change, which is accompanied by muscle fiber atrophy. This fibrosis may obstruct the recovery of atrophied muscle fibers even after reinnervation.

The number of mononuclear interstitial cells increases before fibrotic change in denervated skeletal muscle,[1,2] but labeling peripheral blood cells with radioisotopes demonstrated that the increased interstitial cells were not derived from the circulatory system.[3] These additional interstitial cells have been identified morphologically by electron microscopy as fibroblasts because they have much rough endoplasmic reticulum in their cytoplasm, actin filaments in their processes, and collagen fibers around them.[4]

With the accumulation of interstitial cells in the perisynaptic regions, increased expression of several ECMs such as tenascin-C, fibronectin, neural cell adhesion molecule (N-CAM), and heparan sulfate proteoglycans are observed in denervated skeletal muscle.[5] According to an *in vitro* study, the accumulating interstitial cells are thought to have produced these ECMs.[6] Despite all of these findings, however, whether these interstitial cells are homogeneous or heterogeneous, their definition or identification by cell surface antigens and their roles *in vivo* are still unknown.

Recently, the incorporation of bone marrow-derived cells (BM-DCs), including mesenchymal stem cells[7] or side population cells,[8] into regenerating muscle[9] or dystrophic skeletal muscle[10] was noted. Transplantation of bone marrow cells from GFP transgenic mice allowed the identification of BM-DCs in the recipient mice. Participa-

Supported by the Center of Excellence, Research on Nervous and Mental Disorders (grants-in-aid 10B-1 and 13B-1), the Ministry of Health, Labor, and Welfare of Japan, Research on the Human Genome and Gene Therapy (Health Sciences research grants H10-genome-015 and H13-genome-001), a grant-in-aid for Scientific Research (B) from the Ministry of Education, Science, Sports, and Culture of Japan, and a Research Fellowship from the Japan Society for the Promotion of Science (to K.O.).

Accepted for publication February 15, 2005.

Address reprint requests to Shin'ichi Takeda, MD, PhD, Department of Molecular Therapy, National Institute of Neuroscience, National Center of Neurology and Psychiatry, 4-1-1 Ogawa-higashi-cho, Kodaira, Tokyo 187-8502, Japan. E-mail: takeda@ncnp.go.jp.

tion of BM-DCs was reported not only in the regeneration process, but also in atherosclerotic or fibrotic lesions.[11–13] These findings suggest that regulating migration, homing, proliferation, or differentiation of BM-DCs might lead to mitigation or prevention of these lesions.

To examine whether BM-DCs are also incorporated into pathological processes in skeletal muscle, we studied the origin of the increased interstitial cells in denervated skeletal muscle by using a bone marrow chimeric animal. Here, using GFP bone marrow chimeric mice, we show for the first time that a considerable proportion of these interstitial cells are bone marrow-derived, ie, they are not of traditional fibroblast lineage but of macrophage/monocyte lineage, and that they are a possible regulator of the muscle tissue-derived interstitial cells that might finally constitute the fibrosis.

Materials and Methods

Animals

C57BL/6J mice (B6 mice) and BALB/c mice were purchased from Nihon CLEA (Tokyo, Japan). C57BL/6J-*GFP*-transgenic mice[14] were kindly provided by Dr. Okabe (Osaka University, Japan). All procedures used on experimental animals were approved by the Experimental Animal Care and Use Committee at the National Institute of Neuroscience.

BM Chimeric Mice and Denervation

Whole bone marrow cells were collected from humeri, femurs, and tibias of 7- to 8-week-old donor GFP-transgenic mice by aspiration and flushing. Mononuclear cells were refined through 40-μm and subsequently 10-μm filters and next by centrifugation with Lympholite-M (Cedarlane, Hornby, Ontario, Canada), and then they were diluted to concentrations of 5 to 10 $\times$ 10^6 cells in 100 μl of phosphate-buffered saline (PBS). Female C57BL/6J mice (7- to 8-week old) were lethally irradiated with 9 Gy (Hitachi Medical Co., Tokyo, Japan) immediately before retro-orbital injection of the donor BM cells under general anesthesia with 0.05 mg/g (body weight) of pentobarbiturate (Nembutal). These mice were given drinking water containing 1 mg/ml of ampicillin for 2 weeks after the transplantation.

Twelve weeks after the transplantation, the left sciatic nerve of the bone marrow recipients was excised for nearly the full length of the thigh (approximately 10 mm) from a small incision (approximately 4 mm) made in the mid-lateral thigh under general anesthesia and a surgical microscope (Olympus, Tokyo, Japan). The mice were sacrificed 1 day (day 1) to 4 months (day 112) after denervation by cervical dislocation under general anesthesia. The left gastrocnemius muscle was excised for analysis. The right gastrocnemius muscle served as the control sample. Bone marrow cells simultaneously collected from the femur were purified and then were analyzed by FACS (FACS VantageSE flow cytometer; Falcon, Franklin Lakes, NJ) to determine the bone marrow chimerism as a percentage of GFP-positive cells.

Immunohistochemistry

Muscle samples were fixed with 4% formaldehyde in PBS for 30 minutes and washed with 10% sucrose in PBS for 6 hours and then with 20% sucrose overnight. The samples were then soaked in OCT compound and frozen in isopentane cooled in liquid nitrogen. Serial cryostat sections (10 μm thick) were stained with hematoxylin and eosin (H&E) or immunohistochemically as described below. Sections were washed with PBS for 30 minutes, blocked with 1% bovine serum albumin, and then were reacted with first (37°C, 1 hour) and second (room temperature, 30 minutes) antibodies. Nuclei were stained with TOTO-3 (room temperature, 10 minutes). After staining, the sections were examined under a confocal laser-scanning microscope (Leica TCS SP; Leica, Heidelberg, Germany). To count GFP-positive cells, five randomly selected high-power fields of neuromuscular junction-rich and -poor areas were examined.

Western Blotting Analysis

Twenty to 40 cryostat sections of day 28 or day 112 gastrocnemius muscles were dissolved with 4 volumes (w/v) of sample buffer (10% SDS, 70 mmol/L Tris-HCl (pH 6.7), 10 mmol/L EDTA, and 5% β-mercaptoethanol), boiled for 5 minutes, and then cooled on ice. The samples were centrifuged by 14,500 rpm for 15 minutes, and then the supernatants were collected. The amounts of harvested protein were determined based on OD 595 using Bradford solution. Equal amounts of protein (30 μg each) underwent electrophoresis (200V, 45 minutes) on READYGELS J (7.5%; Bio-Rad, Tokyo, Japan). After semidry blotting was performed (242mA, 1 hour), the membrane was reacted with first (4°C, overnight) and horseradish peroxidase-conjugated second (room temperature, 1 hour) antibodies. The signals were analyzed using Lumi-Imager F1 (Roche Molecular Biochemicals, Tokyo, Japan).

FACS Analysis of Muscle Mononuclear Cells

The visible nerves, blood vessels, and tendons of the whole hind limb muscle of the denervated or intact side were removed with microsurgical forceps under a dissection microscope. Trimmed muscles were minced with scissors and then treated with 0.2% collagenase type 2 under stir for 40 minutes at 37°C. Digested muscles were filtered through a 100-μm and subsequently a 40-μm filter, and then red blood cells were removed by treatment with 0.8% NH_4Cl. The mononuclear cells obtained were suspended in 100 μl of PBS and reacted with antibodies. The first antibody (on ice, 30 minutes) was allophycocyanin-conjugated anti-CD45, phycoerythrin (PE)-conjugated anti-CD11b, or biotin-conjugated anti-CD44. The second reagent for the biotin-conjugated anti-CD44 antibody was PE-conjugated streptavidine (on ice, 15

minutes). Finally, the samples were washed with PBS, dissolved in 1 ml of PBS with 2% bovine serum albumin, and analyzed by FACS.

BrdU Staining

Mice at day 4 were injected intraperitoneally with 50 μg/g body weight of BrdU in 200 μl of PBS. Two hours after the injection,[15] the mice were sacrificed by cervical dislocation. Fixation of the muscle sample was the same as that for immunohistochemistry. Cryostat sections (5 μm thick) were stained with chicken anti-GFP antibody and subsequently fluorescein isothiocyanate-conjugated anti-chicken IgG antibody. Next, after fixation of GFP with 2% formaldehyde, DNA was denatured by 2 N HCl and neutralized by 0.1 mol/L sodium 4-borate (pH 8.5). Then, BrdU staining with anti-BrdU antibody and subsequently Alexa Fluor 568-conjugated goat anti-mouse IgG was performed. The sample was examined under a confocal laser microscope.

Apoptotic Cell Detection

Apoptotic cells were detected on cryostat sections using ApopTag^R Red *In Situ* Apoptosis Detecting kit (Chemicon International Inc.) according to manufacturer's instructions. Briefly, cyostat sections were prepared as described in immunohistochemistry section. Next, GFP staining and fixation was performed as described under BrdU Staining. After being postfixed and permeabilized with pre-cooled (−20°C) mixture of ethanol and acetic acid (2:1), the sections were reacted with digoxigenin-labeled nucleotides under the presence of terminal deoxynucleotidyl transferase. Then, the sections were reacted with rhodamine-conjugated sheep polyclonal anti-digoxigenin antibody. Nuclei were stained with TOTO-3. Sections were examined under a confocal laser microscope.

Reverse Transcriptase-Polymerase Chain Reaction (RT-PCR)

Three fractions of mononuclear cells, GFP positive, GFP negative/CD44 positive, and GFP negative/CD44 negative, from four day 28 mice were isolated by FACS and diluted in PBS. Total RNA from 1 × 10^4 cells of each population was isolated using RNeasy (Qiagen, Tokyo, Japan) according to the manufacturer's instructions and reverse transcribed using oligo dT primers with a total reaction volume of 30 μl. The reverse transcription program was 25°C for 10 minutes, 48°C for 30 minutes, and then 95°C for 5 minutes. Polymerase chain reaction was performed using 3 μl of each RT product (cDNA), with a total reaction volume of 20 μl. The PCR thermal cycle was 94°C for 3 minutes, then 40 cycles (or 30 cycles for transforming growth factor (TGF)-β1) of 94°C for 15 seconds, 60°C for 30 seconds, and 72°C for 30 seconds, and finally 72°C for 5 minutes.

The primers for PCR were type I collagen (413-bp product) sense (5′-GTGAACCTGGCAAACAAGGT-3′) and antisense (5′-CTGGAGACCAGAGAAGCCAC-3′), MMP-14 (308-bp product) sense (5′-ACAAAGATGCCCCCTCAACC-3′) and antisense (5′-GCTTCGTCAAACCAGTGC-3′), MMP-3 (391-bp product) sense (5′-TTCTCCAGGATCTCTGAAGGAGAGG-3′) and antisense (5′-ATTTGGTGGGTTACCACGAGGACATC-3′), tenascin-C (355-bp product) sense (5′-GCCTCAACAACTGCTACAATCGTG-3′) and antisense (5′-TCAGCCCCTGTGAACCCATC-3′), α-smooth muscle actin (α-SMA) (240-bp product) sense (5′-GAGAAGCCCAGCCAGTCG-3′) and antisense (5′-CTCTTGCTCTGGGCTTCA-3′), and TGF-β1 (431-bp product) sense (5′-CTAATGGTGGACCGCAACAAC-3′) and antisense (5′-CGGTTCATGTCATGGATGGTG-3′). These primers were obtained from Qiagen. Primers for β-actin (540-bp product) were sense (5′-GTGGGCCGCTCTAGGCACCAA-3′) and antisense (5′-CTCTTTGATGTCACGCACGATTTC-3′). As positive controls for these primers, RNA samples from 8-week-old mouse mammary gland were used for MMP-3 and from mouse embryo (day 13) were used for the rest.

Antibodies and Chemicals

Collagenase type 2 was from Worthington Biochemical Corp. (Lakewood, NJ). Allophycocyanin-conjugated rat anti-mouse CD45 antibody (clone 30-F11), rat anti-mouse CD31 antibody (clone MO76917), PE-conjugated rat anti-mouse CD11b antibody (clone M1/70), and mouse anti-BrdU antibody (clone MO76134) were from Becton Dickinson (San Diego, CA). Rat biotin-conjugated anti-mouse CD44 antibody (clone KM201) was from Southern Biotechnology Associates, Inc. (Birmingham, AL). Rat anti-mouse laminin-α2 antibody (clone 4H8-2) was from Alexis Corp. (San Diego, CA). Rabbit polyclonal anti-mouse type I collagen antibody (for immunohistochemistry) was from Biogenesis Inc. (Kingston, NH). Rat anti-mouse tenascin-C antibody (clone Mtn12)[16] was kindly provided by Prof. Ekblom (Department of Animal Physiology, Uppsala University, Uppsala, Sweden). Goat polyclonal anti-rat C/EBPα antibody, rabbit polyclonal anti-m-cadherin antibody, goat polyclonal anti-mouse collagen α2 type I antibody (for Western blotting analysis), and rabbit polyclonal anti-human TGF-β1 antibody were from Santa Cruz Biotechnology (Santa Cruz, CA). Rabbit polyclonal anti-human α-SMA antibody was from Lab Vision Corp. (Fremont, CA). Rat anti-mouse N-CAM (clone MAB310) and chicken polyclonal anti-GFP antibody and ApopTag Red *In Situ* Apoptosis Detection kit were from Chemicon International Inc. (Temecula, CA). Alexa Fluor 594-conjugated goat anti-rat IgG antibody, Alexa Fluor 568-conjugated goat anti-rabbit IgG antibody, Alexa Fluor 594-conjugated donkey anti-goat IgG antibody, Alexa Fluor 568-conjugated goat anti-mouse IgG antibody, Alexa Fluor 594-conjugated α-bungarotoxin, and TOTO-3 iodide (642/660) were from Molecular Probes (Eugene, OR). Fluorescein isothiocyanate-conjugated donkey polyclonal anti-

chicken IgG antibody was from Jackson Immuno Research Laboratories (West Grove, PA). Horseradish peroxidase-conjugated rabbit anti-goat IgG antibody was from Zymed Laboratories Inc. (San Francisco, CA). The RNeasy Micro kit was from Qiagen.

TaqManR Reverse Transcription Reagents were from Roche Molecular Systems, Inc. (Branchburg, NJ). The Mouse β-actin Control Amplimer set was from CLONTECH Laboratories, Inc. (Palo Alto, CA). ECL Western Blotting Detection Reagents were from Amersham Biosciences (Little Chalfont, Buckinghamshire, United Kingdom).

Statistical Analysis

Results were expressed as means ± SD. For comparison between any two groups, Welch's *t*-test was applied based on results of the data analysis by F-test. A *P* value of less than 0.01 was considered to indicate statistical significance.

Results

Establishment of GFP BM Chimeric Mice

Fifty-three mice received bone marrow transplantation. Of these, 45 mice were sacrificed and analyzed. The mean bone marrow chimerism at the time of sampling was 88.5 ± 7.9%. One mouse died of unknown cause 16 days after the bone marrow transplantation. Five mice were excluded from the study beoause of scar contraction of the hind limb due to irradiation. Two mice died of deep anesthesia.

Muscle Fiber Atrophy, Increased Interstitial Cells, and Fibrosis in Denervated Muscle

To verify the condition of denervation, the decrease of the diameter of gastrocnemius muscle fibers was examined by analyzing immunohistochemical images. On the denervated side (left), the diameter was significantly decreased 4 days after denervation (day 4; Figure 1). Denervation was also ascertained by observation of separate unconnected stumps of the cut sciatic nerve. On H&E stain, an increase in the number of interstitial mononuclear cells was observed from day 4. They accumulated in perisynaptic regions, as reported in the literature.[1,2]

From day 14, progressive fibrosis was detected by H&E staining. Fibrotic change was also examined by immunostaining for type I collagen (Figure 3, c and d). Fatty change was not observed in C57BL/6J mice, at least up to 4 months after the denervation (day 112). In contrast, the hind limb muscles of BALB/c mice showed fatty change from 1 month after denervation (day 28; data not shown). This difference in phenotypic expression may be interpreted as the influence of background strain.

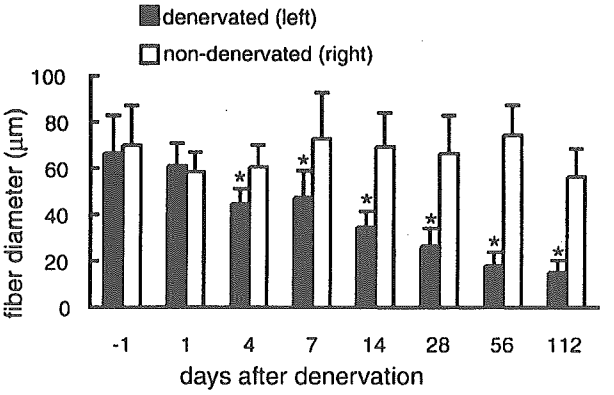

Figure 1. Decrease of muscle fiber diameter in denervated muscle. Diameters of muscle fibers of both denervated (**left, gray bar**) and nondenervated (**right, white bar**) gastrocnemius muscle were measured before denervation (−1) and 1 to 112 days after denervation. Bars represent the means ± SD of 50 fibers. $^{*}P < 0.01$.

BM-DCs Accumulated in the Perisynaptic Region

On day 4, many GFP-positive BM-DCs had entered the denervated (left) gastrocnemius muscle, mainly at the external fascia and perimysium (Figure 2, a and b). BM-DCs then faded out of these regions from day 7, but at the same time they appeared on the endomysium of each muscle fiber and gradually accumulated in the perisynaptic regions (Figure 3a). The time course of the appearance of BM-DCs in the perisynaptic region is shown in Figure 4, a and b. From day 4, BM-DCs significantly increased in the perisynaptic region to reach a maximum around days 14 to 28; thereafter, they gradually decreased. The initial accumulation at the perimysium on day 4 was excluded from this analysis. Distortions in the arrangements and decreases in the number of NMJs were also observed from 2 months after the denervation (day 56) and were more apparent on day 112 (Figure 3b).

When we compared the high-magnification fluorescent images of BM-DCs with that of H&E staining, BM-DCs accounted for considerable part of the interstitial mononuclear cells (Figure 2, c and d). Quantitative analysis showed that BM-DCs accounted for around 43% of the interstitial cells on day 4, 41% on day 14, and 39% on day 28, respectively (Figure 5a). However, as long as we considered only the shape of these increased interstitial cells, BM-DCs and muscle tissue-derived cells (MT-DCs) were indistinguishable under the microscope, and they were spindle or stellate shaped, as reported in the literature.[4]

BM-DCs Co-Localized with Expression of ECMs

Some fibrosis-related components of ECMs are known to accumulate around the perisynaptic regions of denervated skeletal muscle.[5] We examined whether BM-DCs co-localize with expressions of some components of ECMs. Type I collagen was detected in the perisynaptic regions in which BM-DCs were also accumulated (Figure 3, c and d). The accumulation of type I collagen was in

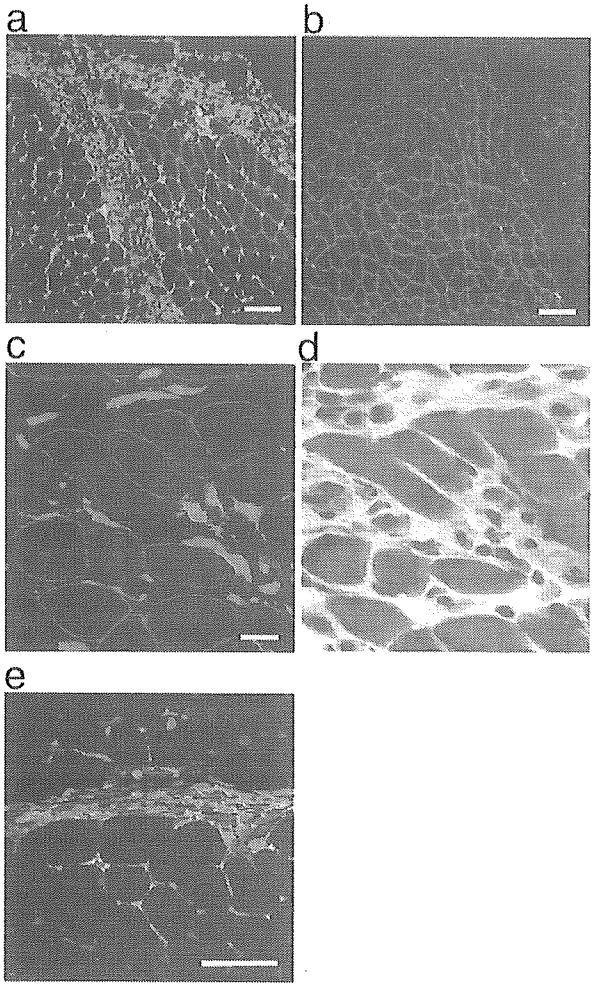

Figure 2. BM-DC infiltration into denervated muscle and co-localization with ECMs. Analysis by immunohistochemistry and H&E. **a:** Many BM-DCs (green; GFP) had infiltrated the external fascia and perimysium (green bands) and spread into the endomysium of denervated gastrocnemius muscle 4 days after denervation (day 4), whereas the nontreated side (**b**) showed no increase of BM-DCs (red; laminin-α2 representing basement membrane). Comparison at high magnification of GFP-positive cells (**c**; green) with interstitial mononuclear cells in H&E (**d**) shows that BM-DCs account for considerable part of the interstitial cells. **e:** Expression of tenascin-C (red) on day 4 at the perimysium, at which the BM-DC (green or merged with nucleus to light blue) accumulated. Within the perimysium, mononuclear MT-DCs (spindle-shaped areas with nuclei, lacking red signal) are also observed. TOTO-3 (dark blue) was used for nuclear staining. Scale bars = 100 μm (**a** and **b**), 20 μm (**c**), and 40 μm (**e**).

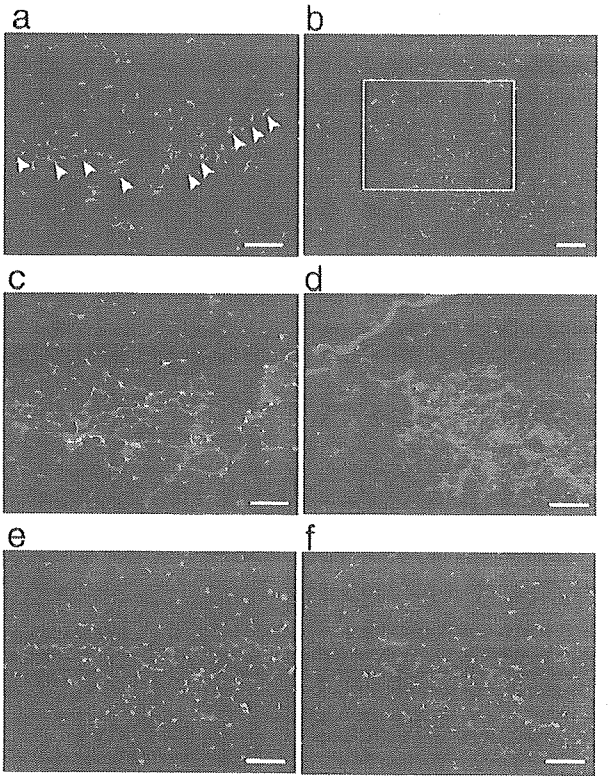

Figure 3. Accumulation of BM-DCs in the perisynaptic region and their co-localization with ECMs. Immunohistochemical analysis of day 28 (**a**, **c**, and **e**; serial sections) and day 112 (**b**, **d**, and **f**; serial sections). BM-DCs accumulated in the perisynaptic regions (**a** and **b**), co-localizing with type I collagen (**c** and **d**, red). BM-DCs also co-localized with tenascin-C on day 28 (**e**, red). Tenascin-C revealed spotted pattern on day 112, although still associating with BM-DCs (**f**, red). **Arrowheads** in **a** indicate individual NMJs (α-bungarotoxin, red). The box in **b** corresponds to the fields of **d** and **f**. Scale bars = 80 μm (**a** and **c** to **f**) and 100 μm (**b**).

accordance with the progressive fibrosis observed in H&E staining. However, immunoblotting analysis showed no evidence that total type I collagen protein had been increased in denervated entire gastrocnemius muscle compared with that of intact side (data not shown). Thus, even if there is increased synthesis of type I collagen in fibrotic lesion in denervated skeletal muscle, degradation of type I collagen may also be involved in the pathogenesis of fibrosis.[17]

The expression of tenascin-C, an anti-adhesion molecule, also accompanied the distribution of BM-DCs and appeared in the perisynaptic regions. On day 4, tenascin-C was detected around the invading BM-DCs or MT-DCs at the perimysium (Figure 2e). On day 7, tenascin-C disappeared from the perimysium, and BM-DCs also disappeared. After day 7, tenascin-C was again detected at the perisynaptic regions in which BM-DCs also accumulated (Figure 3e). This accumulation of tenascin-C might support the idea that tenascin-C appears at sites to which cells migrate, such as development, inflammation, tumorigenesis, and wound healing.[18] However, the expression pattern of tenascin-C was more distinctly restricted to each NMJ than that of type I collagen, especially on day 112 (Figure 3f). Thus, tenascin-C may initially regulate accumulation of BM-DCs at the perimysium, then in perisynaptic regions, and thereafter control, for example, the dynamic induction of regenerating axons to each NMJ. On the other hand, N-CAM[6] was uniformly distributed at each endomysium from day 4, showing no particular co-localization with BM-DCs (data not shown).

There is a possibility that BM-DCs can differentiate into particular cell lineages. Therefore, we examined several typical lineage markers. α-SMA is a marker for myofibroblasts or activated interstitial cells found in inflammatory or chronic lesions. The expression of α-SMA was not detected among BM-DCs and MT-DCs (data not shown). Whether BM-DCs incorporate into satellite cells in skeletal muscle is currently controversial.[19,20] In the present

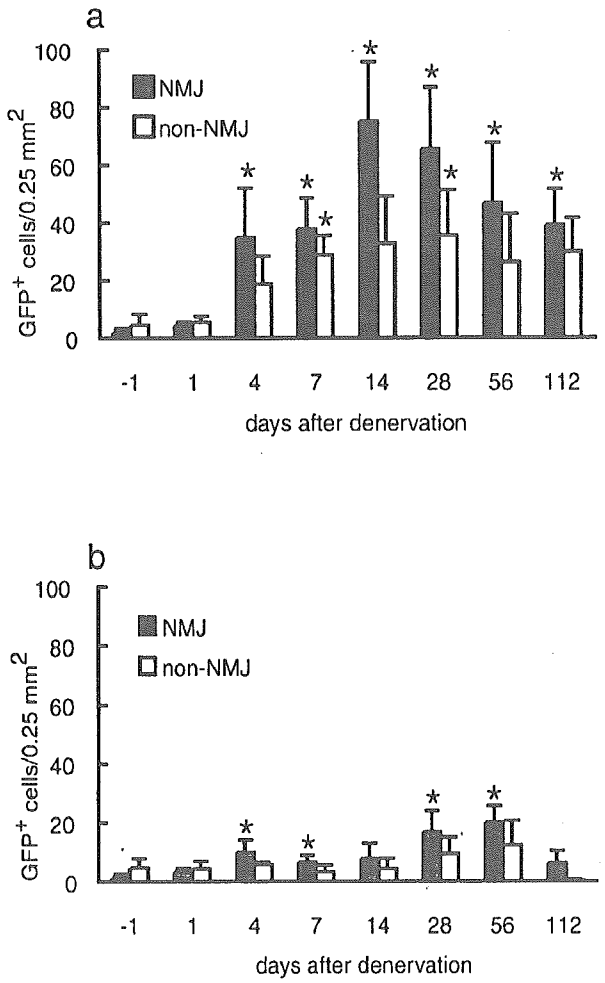

Figure 4. Increase of the BM-DCs in denervated gastrocnemius muscle. Time course of the BM-DC increase in left denervated (**a**) or right nontreated (**b**) side. Data are shown as numbers of GFP-positive cells per field (0.25 mm^2) including (**gray bars**) or excluding (**white bars**) NMJ regions. Bars represent the means ± SD of five fields. $^*P < 0.01$.

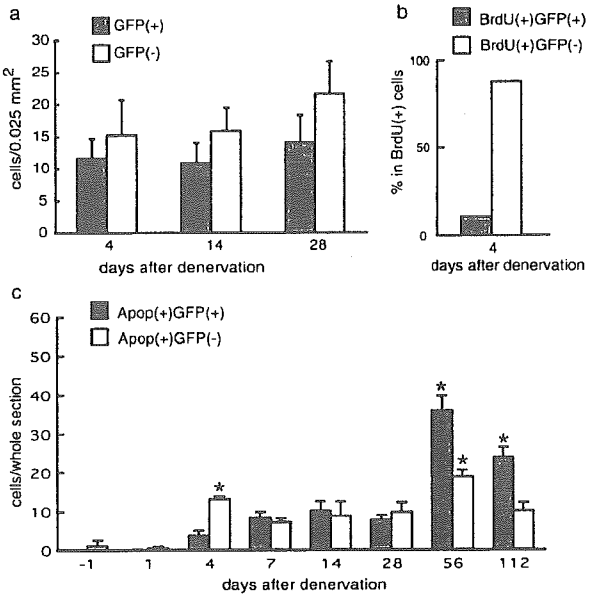

Figure 5. The ratio of BM-DCs among interstitial mononuclear cells in denervated gastrocnemius muscle and their proliferation or apoptotic activity. **a:** Numbers of BM-DCs (**gray bars**) and MT-DCs (**white bars**) around NMJs of denervated muscle. Data are shown as cell numbers per field (0.025 mm^2/field). Interstitial connective tissue was defined as tissue outside the muscle fiber basement membrane stained by laminin-α2. Mononuclear cells were defined by nuclear staining with TOTO-3. **b:** The proportion of interstitial cells (**gray bar**, GFP positive; **white bar**, GFP negative) that were BrdU positive after 2 hours of BrdU exposure in a whole cross-sectional area of gastrocnemius muscle 4 days after denervation. **c:** Time course of apoptotic activity of BM-DCs (**gray bars**) and MT-DCs (**white bars**) of denervated muscle. Data are shown as numbers of apoptotic (Apop) cells per whole muscle section. Bars represent the means ± SD of five fields (**a**) or three whole sections (**c**), respectively. $^*P < 0.01$.

study, GFP-positive satellite cell was not detected in denervated muscle. None of the other lineage markers tested, including CD31 (platelet/endothelium cell adhesion molecule-1) for vascular endothelium, neonatal myosin heavy chain for developing myofibers, and C/EBP-α for adipose cells, was detected among those interstitial cells. Thus, BM-DCs were revealed to be negative for some typical lineage markers, although sparing the possibility that they are fibroblasts.[21]

GFP-positive BM-DCs were also observed in gastrocnemius muscles of the intact side or bilateral nondenervated muscle (Figure 4, a and b). Inappropriate homing of hematopoietic or mesenchymal stem cells resulting from peripheral intravenous injection of bone marrow cells may have caused the survival of these cells. These cells may also reflect the existence of migrant, but long-term-resident, muscle interstitial cells. However, significant increase of BM-DCs in the intact side (Figure 4b) may due to sensitization via denervated leg.

BM-DCs in Denervated Skeletal Muscle Had Monocyte/Macrophage Phenotype

To investigate whether BM-DCs retain a hematopoietic lineage even in denervated skeletal muscle, we tested them for CD45 and CD11b by FACS analysis of total mononuclear cells harvested from whole denervated muscle and by immunohistochemistry of corresponding samples. On FACS analysis, at least up to day 28, the GFP-positive population was revealed to be CD45- and CD11b-positive (Figure 6, a and b). These results again showed that BM-DCs have not *trans*-differentiated into a nonhematopoietic lineage, including fibroblastic, angiogenic, myogenic, adipogenic, or neurogenic lineage, but are fundamentally of monocyte/macrophage lineage.

Next, we tried to define the migrating nature of the increased interstitial cells including BM-DCs and mononuclear MT-DCs by their CD44 expression. CD44 is an adhesive molecule known as an ECM (hyaluronan) receptor[22] that is broadly expressed on the surface of hematopoietic[23] and nonhematopoietic cells of vertebrates. CD44 is involved in lymphocyte homing, macrophage or lymphocyte activation, and tumor metastasis.[24–26] CD44 connects actin filaments with MMP-14 (membrane type 1-MMP; MT1-MMP), which is a representative of membrane type MMP,[27] or activates proMMP-2 at the forward processes (lamellipodia) of such migrating cells.[28] Put together, we expected the

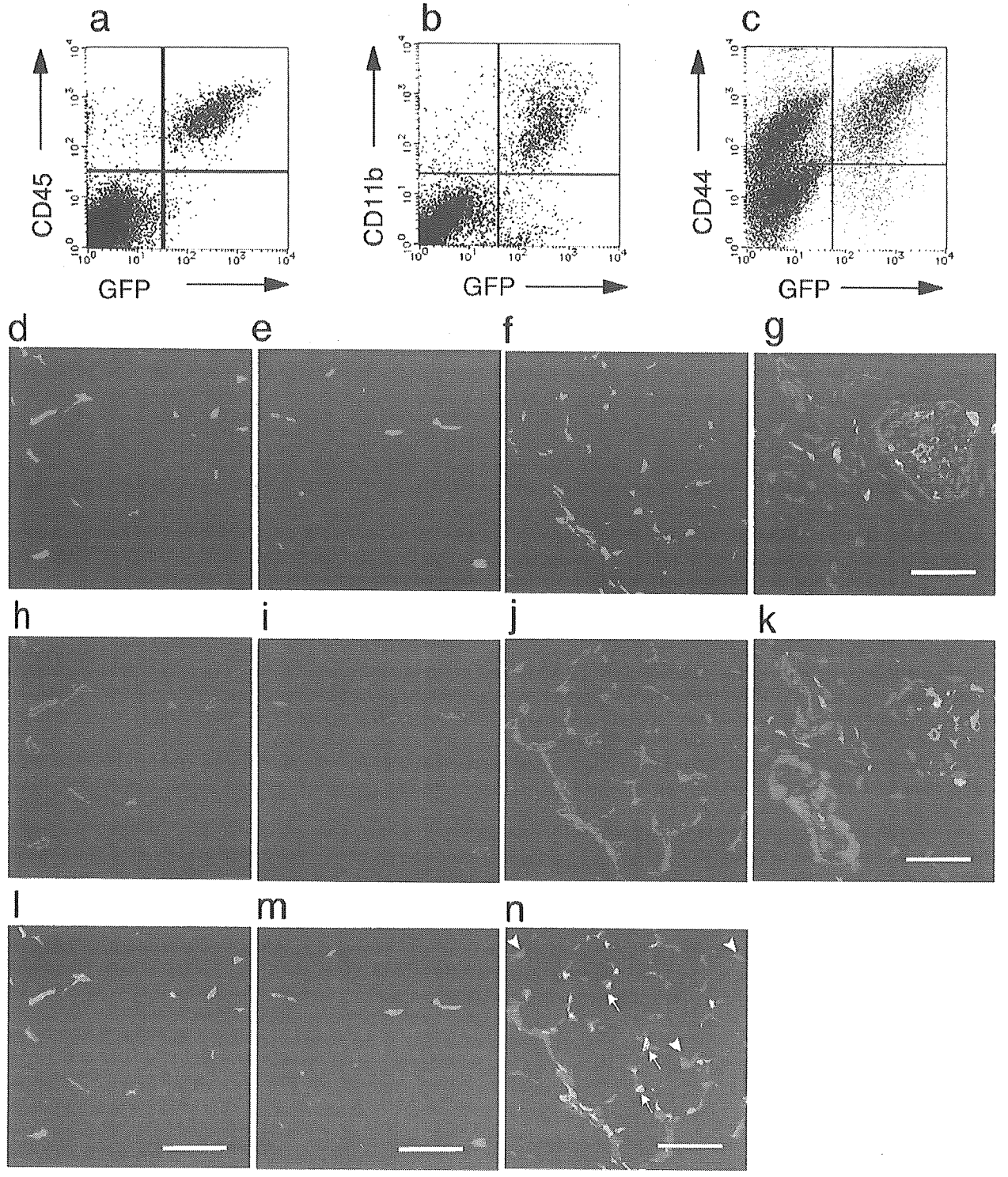

Figure 6. Flow cytometric and immunohistochemical analysis of increased mononuclear interstitial cells in denervated muscle. **a** to **c:** Mononuclear cells were isolated from gastrocnemius muscle 4, 14, and 28 days after the denervation. Following appropriate immunostaining, the cells were analyzed by flow cytometry. Representative results of analysis of isolated mononuclear cells 4 days after the denervation for GFP and CD45 (**a**), CD11b (**b**), and CD44 (**c**). **d** to **n:** Immunohistochemical analysis of BM-DCs in gastrocnemius muscle 14 days after the denervation. Almost all GFP-positive cells (**d** to **f**; green) co-stained with CD45 (**h**; red) and CD11b (**i**, red) and therefore revealed a merged expression pattern for these antigens (**l** and **m**; merged into yellow). On the other hand, CD44-positive cells (**j**; red) were GFP positive (**f**, **j**, and **n**; **arrows**) or GFP negative (**f**, **j**, and **n**; **arrowheads**). **g** and **k:** Serial sections of a neuro-vascular bundle in a gastrocnemius muscle 4 days after denervation stained for CD44 (**g**; red) or α-SMA (**k**; red). TOTO-3 (blue) was used for nuclear staining. Scale bars = 40 μm.

increased mononuclear interstitial cells migrating to the perisynaptic regions to be CD44 positive whether they were BM-DCs or MT-DCs. Accordingly, CD44-positive mononuclear cells contained both GFP-positive and GFP-negative fractions (Figure 6c, top right and top left fractions, respectively). These fractions were supposed to reflect BM-DCs and mononuclear MT-DCs, respectively.

Immunohistochemical analysis supported those findings. Almost all BM-DCs were CD45 positive up to 2 months after the denervation (day 56; Figure 6, d, h, and l) and CD11b positive at least up to 4 months after the denervation (day 112) (Figure 6, e, i, and m, respectively). In addition, almost all interstitial mononuclear cells that might include BM-DCs and mononuclear MT-DCs were positive for CD44 at least up to day 112 (Figure 6, f, j, and n).

Observation of the posterior tibial artery revealed that vascular endothelial cells are CD44 negative (Figure 6, g and k). However, the tibial nerve trunk contained CD44-positive but GFP-negative cells, which were revealed to be Schwann cells by comparing them with a serial section stained with S-100 protein (Figure 6g; data not shown). Some of the large GFP-positive cells observed within the nerve trunk in Figure 6g may be macrophages that are involved in phagocytosis of degenerated axons.[15] Combining the mononuclear cell count with the fractional percentile of FACS-gated cells suggested that the denervated (left) gastrocnemius muscle contained around three to four times as many BM-DCs by muscle weight than the nondenervated (right) side (data not shown).

Poor Proliferation Activity of BM-DCs

There is a possibility that the GFP-positive cells observed in the denervated gastrocnemius muscle originated from muscle tissue-derived GFP-positive interstitial cells: long-term residents of skeletal muscle were found in the nondenervated side. In addition, the increase of the GFP-positive cells may depend on their proliferation by dividing or on a constant supply from the circulation system.

To answer these questions, we performed BrdU staining of denervated gastrocnemius muscle on day 4, the time point of the maximum reported proliferation activity of the increased interstitial cells.[2,3] GFP-positive interstitial cells formed only a very small minority of the BrdU-positive population in the denervated gastrocnemius muscle of day 4 (Figure 5b). Because GFP-positive cells accounted for nearly half of the increased interstitial cells in denervated gastrocnemius muscle on day 4 (Figure 5a), this result suggests poor proliferation potential of the GFP-positive population. Taking only the short life span of blood cells into consideration, it is further suggested that the majority of the increased GFP-positive cells in denervated muscle are not muscle tissue-derived dividing cells but are a bone marrow-derived and continuously supplied population.

Contribution of Apoptosis to the Decrease in Number of BM-DCs

The gradual decrease in number of BM-DCs in denervated gastrocnemius muscle observed from day 28 may be due to decreased circulating-in, increased re-circulating, or increased apoptotic activity of BM-DCs. To assess the contribution of apoptosis to the decrease in number of BM-DCs, we performed quantitative analysis of apoptotic cells in denervated gastrocnemius muscle. GFP-positive apoptotic cells significantly increased in number from day 56 ($P < 0.01$; Figure 5c). The result suggests that increased apoptotic activity of BM-DCs contributed to the gradual decrease in number of BM-DCs in denervated skeletal muscle. Although implication of the increased apoptotic activity of GFP-negative cells (MT-DCs) on day 4 (Figure 5c) is unclear, apoptotic activity of MT-DCs generally followed that of BM-DCs, indicating cooperative cellular rolls among these populations.

BM-DCs Expressed TGF-β1

To distinguish the functional roles of BM-DCs and MT-DCs, we studied the gene expression patterns of these populations by RT-PCR (Figure 7a). Denervated skeletal muscle of day 28 mice was chosen because many BM-DCs had accumulated in the perisynaptic region at the date. As controls, bilateral intact hind limb muscles of bone marrow chimeric mice were used instead of those of the contra-lateral side of the denervated limb to exclude the possibility of any compensative up- or down-regulation of the genes.

In denervated muscle, the CD44-positive MT-DCs, which may reflect muscle tissue-derived mononuclear cells and Schwann cells (as shown in Figure 6g), mainly expressed type I collagen and tenascin-C, suggesting that this population contains fibroblasts as the main effector of fibrosis (Figure 7a, lane 2). In contrast, BM-DCs did not express type I collagen or tenascin-C; instead, they dominantly expressed TGF-β1, a principal growth factor known to promote fibrosis in persistent inflammation or to induce the synthesis of tenascin-C *in vitro* (Figure 7a, lane 1).[29] Immunohistochemical analysis showed dominant production of TGF-β1 protein by a portion of BM-DCs (Figure 7, b to d). TGF-β1 expressions by the CD44-positive MT-DCs, which potentially include fibroblasts, were not observed by RT-PCR (Figure 7a, lane 2) or immunohistochemically. However, slight to moderate amplification of TGF-β1 was detected from MT-DCs when PCR was performed by 40 cycles, in accordance with the common establishment that virtually all fibroblasts express TGF-β1 (data not shown). Despite being considered to only reflect vascular endothelial cells as shown in Figure 6k and therefore to express no particular molecules studied here, the CD44-negative MT-DCs also expressed type I collagen and tenascin-C (Figure 7a, lane 3).

We examined whether MMP- 3 (stromelysin-1), one of the soluble MMPs known to breakdown the largest variety

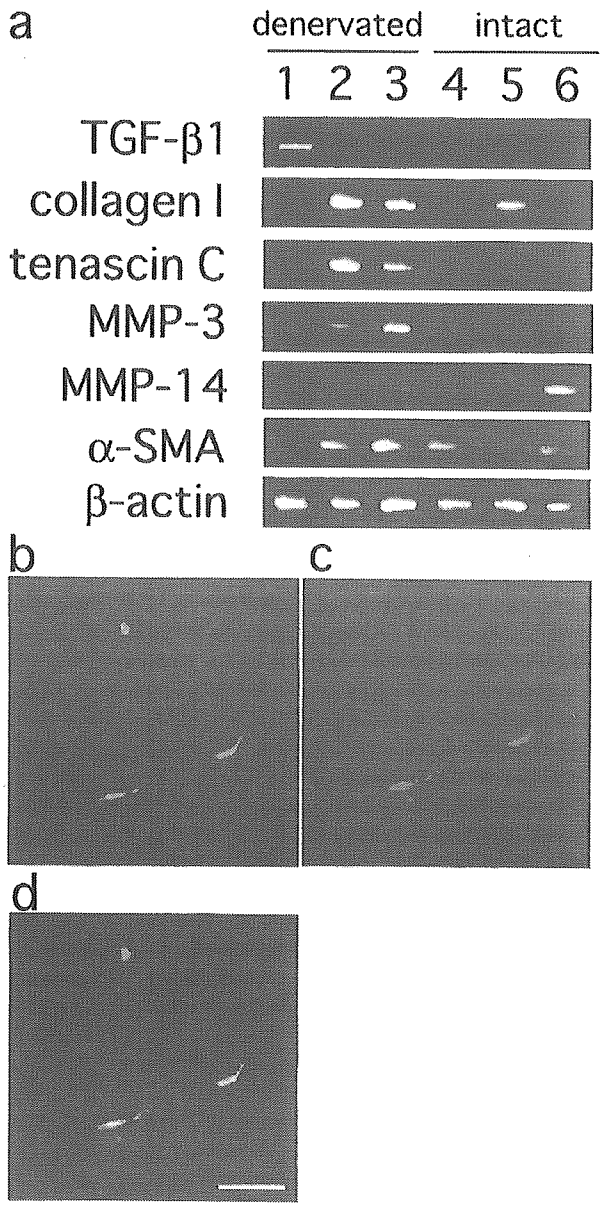

Figure 7. Expression patterns of fibrosis-related molecules within increased mononuclear interstitial cells in denervated muscle. **a:** RT-PCR analysis of fibrosis-related molecules of increased mononuclear interstitial cells in denervated muscle fractionated by FACS. Mononuclear interstitial cells were isolated from gastrocnemius muscle from either four mice 28 days after the denervation or intact mice. After appropriate immunostaining, approximately 1×10^4 cells in each fraction of GFP positive (**lanes 1** and **4**), GFP negative/CD44 positive (**lanes 2** and **5**), and GFP negative/CD44 negative (**lanes 3** and **6**) were collected by flow cytometry (corresponding to upper right, upper left, and lower left fractions in Figure 6c, respectively). After mRNA extraction from collected cells, RT-PCR was performed. Denervated mice (**lanes 1** to **3**), intact mice (**lanes 4** to **6**). **b** to **d:** Immunohistochemical detection of TGF-β1 protein in day 28 denervated gastrocnemius muscle. A portion of GFP-positive cells (**b**; green) co-stained with TGF-β1 at their cytoplasm (**c**; red) and therefore revealed a merged expression pattern (**d**; merged into yellow). Scale bars = 40 μm.

of substrates including gelatin, was expressed in the denervated muscle. MMP-3 is known to activate morphogenesis,[30] epithelial-to-mesenchymal conversion,[31] and carcinogenesis[32] of the mammary gland. MMP-3 was clearly detected in the denervated side especially in CD44-negative fraction (Figure 7a, lane 3). Although MMP-14 is reported to interact with CD44 on migrating cells,[27] less amplification of MMP-14 was detected in denervated muscle than in intact muscle. Further paradoxically, MMP-14 tended to be expressed in CD44-negative fraction (Figure 7a, lanes 3 and 6).

In MT-DCs of intact muscle, α-SMA was mainly expressed by CD44-negative fraction, probably reflecting vascular wall cells (Figure 7a, lane 6). In denervated muscle, both CD44-positive and -negative fractions showed up-regulation of α-SMA. This result may indicate an enhanced myofibroblastic phenotype in MT-DCs due to denervation, although α-SMA was not detected well among them immunohistochemically (Figure 7a, lanes 2 and 3). In denervated muscle, BM-DCs did not express α-SMA (Figure 7a, lane 1). Interestingly, BM-DCs did express α-SMA in intact muscle (Figure 7a, lane 4). Because BM cells were injected intravenously when establishing BM chimera, some of them, especially those that potentially express α-SMA, might have inappropriately homed into skeletal muscle. Therefore, such α-SMA-positive cells might, if small in number, occupy considerable proportion of BM-DCs in intact muscle, whereas α-SMA-negative migrant monocytes/macrophages might account for the majority of BM-DCs in denervated muscle. Thus, α-SMA may have been detected from BM-DCs in intact muscle and not in denervated muscle by analyzing the equal number of cells.

On the innervated side, very slight amplification of TGF-β1 expressed by BM-DCs was observed (Figure 7a, lane 4). Slight to moderate amplifications of type I collagen and tenascin-C were also observed in CD44-positive and -negative populations (Figure 7a, lanes 5 and 6). These signals may in general reflect the baseline or normal expressions of these genes.

Discussion

In this study, we proved that a great number of BM-DCs accounted for the increased number of interstitial cells in denervated skeletal muscle, in contrast to a previous study,[3] which concluded that the increased interstitial cells were derived from muscle tissue. In the experiment, white blood cell precursors were pre-labeled by repeated injection of titrated thymidine ([^{3}H]TdR) into subcutis of 7-to 10-week-old male albino mice 6 or 2 days before denervation. Determination of the presence of labeled leukocytes in denervated and control muscles was made 3 or 4 days after denervation by scintillation counting of muscle homogenates. As a consequence, incorporation of circulating-in cells into denervated extensor digitorum longus seemed unlikely in their study, although one of their time points of sampling was similar to one of those in our present study (day 4), on which an increased number of BM-DCs was observed. In contrast, bone marrow-chimeric animal enabled us to directly label bone marrow cells including mesenchymal stem cells and hematopoietic stem cells, to label peripheral leukocytes sufficiently, and to identify individual labeled cells. Thus, the negative result in the previous study for incorporation of BM-DCs

into denervated muscle may be due to technical limitations in labeling peripheral blood cells by radioisotopes or in detecting them.

Although the increased interstitial cells in denervated muscle have been currently identified as fibroblasts by electron microscopy, further intensive comparison of electron-microscopic images with that of the serial GFP fluorescent sections or immuno-electron microscopic study might enable observation of a distinction between BM-DCs and MT-DCs, bringing a novel morphological identification of these populations.

Evidence is emerging that BM-DCs play significant roles in fibrosis of other organs after progressive inflammation or injury. In pulmonary fibrosis, the majority of collagen-producing fibroblasts turned out to be bone marrow derived.[13,33] In renal fibrosis, about 14% to 15% of fibroblasts were bone marrow-derived,[12] in addition to the bone marrow monocytes that contribute to the growing process of fibrosis by facilitating the epithelial-mesenchymal transition.[34] In liver fibrosis, BM-DCs accounted for up to 22.2% of myofibroblasts: cells positive for α-SMA and vimentin and negative for CD45.[35]

In contrast, our results suggested that BM-DCs in denervated skeletal muscle were of a monocyte/macrophage lineage and therefore were not fibroblasts by definition of lineage-specific cell surface antigen, whereas that MT-DCs might contain fibroblasts. Thus, BM-DCs in denervated muscle were revealed not to differentiate into fibroblasts, as reported in fibrosis of some vital organs, but instead to maintain their monocyte/macrophage lineage. This inconsistency in the role of BM-DCs can be explained by the possibility that the pathology of denervated skeletal muscle is different from that of progressive inflammation in response to tissue injury. The increased interstitial cells in denervated muscle exhibited an anatomically characteristic distribution: they accumulated in perisynaptic regions of the denervated muscle. Interestingly, not only this accumulation but also the increase of interstitial cells itself is absent when the muscle is only immobilized by blocking the motor nerve with tetrodotoxin.[36] In addition, expression of tenascin-C or fibronectin is also undetected in such immobilized muscles.[36] These observations suggest that some signals related to denervation itself trigger the chemotaxis of macrophages to perisynaptic regions. These alterations may include axon degeneration, morphological alterations of Schwann cells around nerve terminals (terminal Schwann cells), and the lack of any substance usually supplied to the NMJ by axonal transport (Figure 8). One of the candidates for the signal factor may be monocyte chemoattractant protein-1 (MCP-1), a prototype of the CC chemokine. Mitigation of fibrosis by inhibiting monocyte infiltration with an MCP-1-blocking antibody or recently, by genetic intervention in the MCP-1 gene have been described in kidney,[37] lung,[38] and blood vessel.[39] Furthermore , MCP-1 is known to be produced by Schwann cells of denervated peripheral nerves and to induce infiltration by macrophages.[40] In denervated muscle, MCP-1 may be restrictedly expressed by terminal Schwann cells around the perisynaptic region and may attract BM-DCs of macrophage/monocyte lineage (Figure 8).

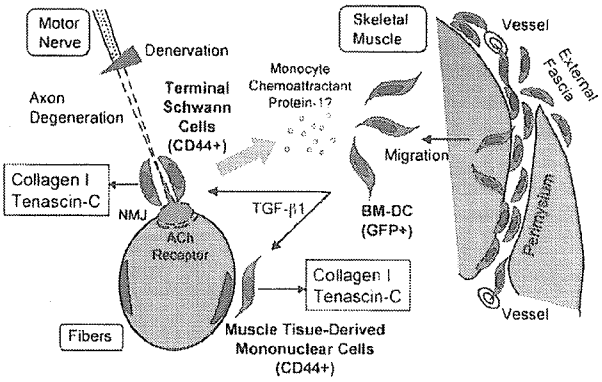

Figure 8. The cellular and molecular mechanisms of fibrosis in denervated skeletal muscle. Denervation-related signals (axon degeneration or cessation of axonal transport, for example) trigger release of chemokines such as MCP-1 from terminal Schwann cells. Circulating cells of macrophage/monocyte lineage originating from bone marrow (BM-DCs) are attracted by them and migrate to the perisynaptic region. The BM-DC release TGF-β1 to stimulate local (muscle tissue-derived) cells including fibroblasts or terminal Schwann cells to produce ECMs including type I collagen or tenascin-C. These ECMs might essentially support preservation of the position of each NMJ or induction of regenerating axons when reinnervated, although an excess of ECMs lead to fibrosis.

We also showed for the first time the gene expression patterns of increased mononuclear interstitial cells in denervated skeletal muscle after dividing them into BM-DCs and MT-DCs by flow cytometric analysis. In contrast to fibrotic changes in some vital organs, BM-DCs never expressed components of ECMs, including type I collagen, in denervated muscle, whereas MT-DCs can be a main source of these ECMs. Instead, BM-DCs dominantly expressed TGF-β1, suggesting the regulatory role of BM-DCs in the fibrotic process (Figure 8). Although cultured fibroblasts isolated from denervated muscle were reported to express tenascin-C, those fibroblasts acquired the potential to produce it.[6] In addition, those "fibroblasts" might have contained other kinds of cells, including BM-DCs.

To determine functions of MT-DCs, we tried to clarify gene expression patterns of mononuclear interstitial cells by analyzing CD44-positive MT-DCs. Although all visible nerves and vessels, as shown in Figure 6, g and k, were removed before the samples were processed, immunohistochemical analysis suggested that the CD44-positive fraction possibly contained Schwann cells. One possible function of CD44 on Schwann cells is regulation of withdrawal of the myelin sheath from degenerated axons. The other possibility is that CD44 may support the connection of Schwann cells, especially perisynaptic ones (terminal Schwann cells), to muscle fibers at the position of the NMJ before denervation. This possibility may include the idea that Schwann cells also express type I collagen or tenascin-C themselves to hold their positions when denervated (Figure 8).

In the denervated side, not only the CD44-positive population but also the CD44-negative population expressed both type I collagen and tenascin-C, although these components of ECMs were more clearly detected in the CD44-positive population than in the CD44-nega-

tive population. Thus, the CD44-negative population may contain populations reactive to denervation. These may include muscle spindle cells, smooth muscle cells, vascular pericytes, perineural cells, and satellite cells. Some of these cells may express those components of ECMs or specifically express MMP-3 when denervated.

In conclusion, bone marrow-derived cells are suggested to regulate the pathogenetic process of fibrosis in denervated skeletal muscle. We believe that further investigation of the nature of BM-DCs will provide a novel approach that may lead to establishment of therapeutic amelioration of excessive fibrosis not only of denervated skeletal muscle but also of fatal neuromuscular disorders including amyotrophic lateral sclerosis as well as the latest investigations of fibrosis in other vital organs.

Acknowledgments

We are grateful to colleagues in our laboratory, in particular Dr. S. Fukada, for useful discussion and suggestions on this work.

References

1. McGeachie J, Allbrook D: Cell proliferation in skeletal muscle following denervation or tenotomy. Cell Tiss Res 1978, 193:259–267
2. Murray MA, Robbins N: Cell proliferation in denervated muscle: time course, distribution and relation to disuse. Neuroscience 1982, 7:1817–1822
3. Murray MA, Robbins N: Cell proliferation in denervated muscle: identify and origin of dividing cells. Neuroscience 1982, 7:1823–1833
4. Connor EA, McMahan UJ, Marshall RM: Cell accumulation in the junctional region of denervated muscle. J Cell Biol 1987, 104:109–120
5. Sanes JR, Schachner M, Covault J: Expression of several adhesive macromolecules (N-CAM, L1, tenascin (J1), NILE, uvomorulin, laminin, fibronectin, and a heparan sulfate proteoglycan) in embryonic, adult, and denervated adult skeletal muscle. J Cell Biol 1986, 102:420–431
6. Gatchalian CL, Schachner M, Sanes JR: Fibroblasts that proliferate near denervated synaptic sites in skeletal muscle synthesize the adhesive molecules tenascin (J1), N-CAM, fibronectin, and a heparan sulfate proteoglycan. J Cell Biol 1989, 108:1873–1890
7. Pereira RF, Halford KW, O'Hara MD, Leeper DB, Sokolov BP, Pollard MD, Bagasra O, Prockop DJ: Cultured adherent cells from marrow can serve as long-lasting precursor cells for bone, cartilage, and lung in irradiated mice. Proc Natl Acad Sci USA 1995, 92:4857–4861
8. Zhou S, Schuetz JD, Bunting KD, Colapietro AM, Sampath J, Morris JJ, Lagutina I, Grosveld GC, Osawa M, Nakauchi H, Sorrentino BP: The ABC transporter Bcrp1/ABCG2 is expressed in a wide variety of stem cells and is a molecular determinant of the side-population phenotype. Nat Med 2001, 7:1028–1034
9. Ferrari G, De Angelis GC, Coletta M, Paolucci E, Stornaiuolo A, Cossu G, Mavilio F: Muscle regeneration by bone marrow-derived myogenic progenitors. Science 1998, 279:1528–1530
10. Gussoni E, Soneoka Y, Strickland CD, Buzney EA, Khan MK, Flint AF, Kunkel LM, Mulligan RC: Dystrophin expression in the mdx mouse restored by stem cell transplantation. Nature 1999, 401:390–394
11. Sata M, Saiura A, Kunisato A, Tojo A, Okada S, Tokuhisa T, Hirai H, Makuuchi M, Hirata Y, Nagai R: Hematopoietic stem cells differentiate into vascular cells that participate in the pathogenesis of atherosclerosis. Nat Med 2002, 8:403–409
12. Iwano M, Plieth D, Danoff TM, Xue C, Okada H, Neilson EG: Evidence that fibroblasts derive from epithelium during tissue fibrosis. J Clin Invest 2002, 110:341–350
13. Hashimoto N, Jin H, Liu T, Chensue SW, Phan SH: Bone marrow-derived progenitor cells in pulmonary fibrosis: J Clin Invest 2004, 113:243–252
14. Okabe M, Ikawa M, Kominami K, Nakanishi T, Nishimune Y: 'Green mice' as a source of ubiquitous green cells. FEBS Lett 1997, 407:313–319
15. Mueller M, Leonhard C, Wacker K, Ringelstein EB, Okabe M, Hickey WF, Kiefer R: Macrophage response to peripheral nerve injury: the quantitative contribution of resident and hematogeneous macrophages. Lab Invest 2003, 83:175–185
16. Talts JF, Eng H, Zhang HY, Faissner A, Ekblom P: Characterization of monoclonal antibodies against tenascin-C: no apparent effect on kidney development in vitro. Int J Dev Biol 1997, 41:39–48
17. Savolainen J, Myllyla V, Myllyla R, Vihko V, Vaananen K, Takala TE: Effects of denervation and immobilization on collagen synthesis in rat skeletal muscle and tendon. Am J Physiol 1988, 254:R897–R902
18. Chiquet-Ehrismann R: Tenascins, a growing family of extracellular matrix proteins. Experientia 1995, 51:853–862
19. LaBarge MA, Blau HM: Biological progression from adult bone marrow to mononucleate muscle stem cell to multinucleate muscle fiber in response to injury. Cell 2002, 111:589–601
20. Ojima K, Uezumi A, Miyoshi H, Masuda S, Morita Y, Fukase A, Hattori A, Nakauchi H, Miyagoe-Suzuki Y, Takeda S: Mac-1^{low} early myeloid cells in the bone marrow-derived SP fraction migrate into injured skeletal muscle and participate in muscle regeneration. Biochem Biophys Res Commun 2004, 321:1050–1061
21. Strutz F, Okada H, Lo CW, Danoff T, Carone RL, Tomaszewski JE, Neilson EG: Identification and characterization of a fibroblast marker: FSP1. J Cell Biol 1995, 130:393–405
22. Aruffo A, Stamenkovic I, Melnick M, Underhill CB, Seed B: CD44 is the principal cell surface receptor for hyaluronate. Cell 1990, 61:1303–1313
23. Trowbridge IS, Lesley R, Schulte R, Hyman R, Trotter J: Biochemical characterization and cellular distribution of a polymorphic, murine cell-surface glycoprotein expressed on lymphoid tissues. Immunogenetics 1982, 15:299–312
24. Schmits R, Filmus J, Gerwin N, Senaldi G, Kiefer F, Kundig T, Wakeham A, Shahinian A, Catzavelos C, Rak J, Furlonger C, Zakarian A, Simard JJL, Ohashi PS, Paige CJ, Gutierrez-Ramos JC, Mak TW: CD44 regulates hematopoietic progenitor distribution, granuloma formation, and tumorigenicity. Blood 1997, 90:2217–2233
25. Protin U, Schweighoffer T, Jochum W, Hilberg F: CD44-deficient mice develop normally with changes in subpopulations and recirculation of lymphocyte subsets. J Immunol 1999, 163:4917–4923
26. Naot D, Sionov RV, Ish-Shalom D: CD44: structure, function, and association with the malignant process. Adv Cancer Res 1997, 71:241–319
27. Mori H, Tomari T, Koshikawa N, Kajita M, Itoh Y, Sato H, Tojo H, Yana I, Seiki M: CD44 directs membrane-type 1 matrix metalloproteinase to lamellipodia by associating with its hemopexin-like domain. EMBO J 2002, 21:3949–3959
28. Itoh Y, Takamura A, Ito N, Maru Y, Sato H, Suenaga N, Aoki T, Seiki M: Homophilic complex formation of MT1-MMP facilitates proMMP-2 activation on the cell surface and promotes tumor cell invasion. EMBO J 2001, 20:4782–4793
29. Pearson CA, Pearson D, Shibahara S, Hofsteenge J, Chiquet-Ehrismann R: Tenascin: cDNA cloning and induction by TGF-β. EMBO J 1988, 7:2977–2982
30. Wiseman BS, Sternlicht MD, Lund LR, Alexander CM, Mott J, Bissell MJ, Soloway P, Itohara S, Werb Z: Site-specific inductive and inhibitory activities of MMP-2 and MMP-3 orchestrate mammary gland branching morphogenesis. J Cell Biol 2003, 162:1123–1133
31. Lochter A, Galosy S, Muschler J, Freedman N, Werb Z, Bissell MJ: Matrix metalloproteinase stromelysin-1 triggers a cascade of molecular alterations that leads to stable epithelial-to-mesenchymal conversion and a premalignant phenotype in mammary epithelial cells. J Cell Biol 1997, 139:1861–1872
32. Sternlicht MD, Lochter A, Sympson CJ, Huey B, Rougier JP, Gray JW, Pinkel D, Bissell MJ, Werb Z: The stromal proteinase MMP3/stromelysin-1 promotes mammary carcinogenesis. Cell 1999, 98:137–146
33. Dunsmore SE, Shapiro SD: The bone marrow leaves its scar: new concepts in pulmonary fibrosis. J Clin Invest 2004, 113:180–182
34. Sato M, Muragaki Y, Saika S, Roberts AB, Ooshima A: Targeted disruption of TGF-β1/Smad3 signaling protects against renal tubulo-

interstitial fibrosis induced by unilateral ureteral obstruction. J Clin Invest 2003, 112:1486–1494
35. Forbes SJ, Russo FP, Rey V, Burra P, Rugge M, Wright NA, Alison MR: A significant proportion of myofibroblasts are of bone marrow origin in human liver fibrosis. Gastroenterology 2004, 126:955–963
36. Connor EA, Qin K, Yankelev H, DeStefano D: Synaptic activity and connective tissue remodeling in denervated frog muscle. J Cell Biol 1994, 127:1435–1445
37. Wada T, Furuichi K, Sakai N, Iwata Y, Kitagawa K, Ishida Y, Kondo T, Hashimoto H, Ishiwata Y, Mukaida N, Tomosugi N, Matsushima K, Egashira K, Yokoyama H: Gene therapy via blockade of monocyte chemoattractant protein-1 for renal fibrosis. J Am Soc Nephrol 2004, 15:940–948
38. Inoshima I, Kuwano K, Hamada N, Hagimoto N, Yoshimi M, Maeyama T, Takeshita A, Kitamoto S, Egashira K, Hara N: Anti-monocyte chemoattractant protein-1 gene therapy attenuates pulmonary fibrosis in mice. Am J Physiol Lung Cell Mol Physiol 2004, 286:L1038–L1044
39. Gosling J, Slaymaker S, Gu L, Tseng S, Zlot CH, Young SG, Rollins BJ, Charo IF: MCP-1 deficiency reduces susceptibility to atherosclerosis in mice that overexpress human apolipoprotein B. J Clin Invest 1999, 103:773–778
40. Tofaris GK, Patterson PH, Jessen KR, Mirsky R: Denervated Schwann cells attract macrophages by secretion of leukemia inhibitory factor (LIF) and monocyte chemoattractant protein-1 in a process regulated by interleukin-6 and LIF. J Neurosci 2002, 22:6696–6703

A new congenital form of X-linked autophagic vacuolar myopathy

Abstract—In a new family with X-linked congenital autophagic vacuolar myopathy (AVM), seven affected boys presented with congenital hypotonia, dyspnea, and dysphagia with delayed motor milestones. Muscle pathology revealed autophagic vacuoles with sarcolemmal features, multilayered basal lamina with marked sarcolemmal deposition of C5-9 membrane attack complex and calcium, histologically indistinguishable from childhood-onset X-linked myopathy with excessive autophagy (XMEA). Haplotype analysis suggests that this new AVM and XMEA may be allelic despite different clinical presentations.

NEUROLOGY 2005;65:1132–1134

C. Yan, MD; M. Tanaka, PhD; K. Sugie, MD, PhD; T. Nobutoki, MD; M. Woo, MD; N. Murase, MD, PhD; Y. Higuchi, MD, PhD; S. Noguchi, PhD; I. Nonaka, MD, PhD; Y.K. Hayashi, MD, PhD; and I. Nishino, MD, PhD

Autophagic vacuolar myopathy (AVM) is pathologically characterized by presence of autophagic vacuoles with sarcolemmal features (AVSF)—autophagic vacuoles with expression of virtually all sarcolemmal proteins and acetylcholinesterase (AChE).[1] Four forms of AVM with AVSF have been identified: Danon disease,[2] X-linked myopathy with excessive autophagy (XMEA),[3] infantile AVM,[4] and adult-onset AVM with multiorgan involvement.[5] Danon disease is an X-linked dominant disorder with LAMP-2 gene (LAMP-2) mutation on chromosome Xq24 resulting in a triad of skeletal myopathy, hypertrophic cardiomyopathy, and mild mental retardation.[2] XMEA, also known as X-linked vacuolated myopathy,[6] is slowly progressive, with no other organ involvement. Linkage analysis identified the XMEA locus in the most telomeric region of chromosome X.[7] Infantile AVM patients were floppy at birth, with myopathy and cardiomyopathy causing early death.[4] Recently, a patient with adult-onset AVM with multiorgan involvement (eyes, heart, liver, lung, kidney, and skeletal muscles) was reported. In this study, we describe a new Chinese-American family with a severe form of myopathy with AVSF.

From the Department of Neuromuscular Research (Drs. Yan, Tanaka, Sugie, Noguchi, Nonaka, Hayashi, and Nishino), National Institute of Neuroscience, National Hospital for Mental, Nervous and Muscular Disorders (Drs. Nobutoki and Nonaka), National Center of Neurology and Psychiatry, Kodaira, Tokyo; Dr. Woo's Pediatric Clinic (Dr. Woo), Kyoto; Departments of Neurology (Dr. Murase) and Pediatrics (Dr. Higuchi), National Hospital Organization Utano National Hospital, Kyoto, Japan; and Department of Neurology (Dr. Yan), Qilu Hospital of Shandong University, Jinan, China.

Supported partly by the Research on Health Sciences focusing on Drug Innovation and the Research on Psychiatric and Neurologic Diseases and Mental Health from the Japanese Health Sciences Foundation; partly by a Grant-in-Aid for Scientific Research from the Japan Society for the Promotion of Science; and partly by a Research Grant (17A-10) for Nervous and Mental Disorders from the Ministry of Health, Labor and Welfare.

Disclosure: The authors report no conflicts of interest.

Received February 17, 2005. Accepted in final form June 20, 2005.

Address correspondence and reprint requests to Dr. Ichizo Nishino, Department of Neuromuscular Research, National Institute of Neuroscience, National Center of Neurology and Psychiatry, 4-1-1 Ogawa-Higashi, Kodaira, Tokyo 187-8502, Japan; e-mail: nishino@ncnp.go.jp

Methods. All clinical materials used were obtained with informed consent. Genomic DNA was isolated from peripheral lymphocytes using a standard technique. Muscle specimens were flash-frozen in isopentane chilled with liquid nitrogen for histologic analysis or fixed in 2% glutaraldehyde and postfixed in osmium tetroxide for electron microscopic analysis.

Seven male patients in this family presented with similar clinical symptoms (figure 1). Patient IV-2 (figure 1, C and D), a 7-year-old boy from nonconsanguineous Chinese-American parents, had congenital hypotonia and hypoventilation requiring respiratory support for 3 days. Because of difficulty suckling and dysphagia, nasogastric tube feeding was initiated until age 2½ years. The patient's motor milestones were delayed, with sitting at 9 months and walking with support at 2 years. Thereafter, his motor development deteriorated, with progressive muscle weakness and crawling at age 7 years. His serum creatine kinase (CK) level was increased at 1,962 IU/L (reference range = 51 to 197). Generalized muscle atrophy and weakness, including facial and neck muscles, were observed. He had a high-arched palate with normal mentation. EKG revealed incomplete right bundle-branch block, and echocardiography showed left ventricular hypertrophy. Needle EMG of the right biceps brachii revealed complex repetitive discharges without fibrillation potentials or positive sharp waves and low-amplitude, short-duration motor unit potentials with early recruitment, which are compatible with a chronic myopathic condition.

Patient IV-1 (figure 1, B and D) was the 9-year-old elder brother of the proband. He was also hypotonic at birth, with an increased CK level (2,000 IU/L). He also required nasogastric tube feeding until age 2 years. He sat at 8 months and walked at 21 months but became wheelchair bound at age 5 years. He had generalized muscle weakness and atrophy, including facial and neck muscles, with no cardiac or CNS involvement.

Two maternal uncles (III-2 and -3) had asphyxia and died immediately after birth. Another maternal uncle (III-5) had a weak cry and died at age 8 months. Two maternal grandmother's brothers (II-3 and -4) died within several months after birth because of difficulty suckling. No female relatives had clinical signs of myopathy, including the mother (III-4) of the index patients, with a normal CK level (39 IU/L).

Haplotyping and linkage analysis. Haplotype analysis of the genomic DNA from two affected (IV-1 and IV-2) and six unaffected family members (I-2, II-1, II-2, III-1, III-4 and III-6) (see figure 1) was performed using an ABI PRISM 310 genetic analyzer (PE Applied Biosystems, CA) with the following 23 microsatellite markers on chromosome X: Xpter-DXS1060-DXS8051-DXS987-DXS1226-DXS121-DXS1068-DXS993-DXS991-DXS986-DXS990-DXS458-DXS1106-DXS8096-DXS8055-DXS1001-DXS1047-DXS691-DXS1227-DXS8043-DXS1215-DXS8091-DXS8069-DXS1073-Xqter. The multipoint linkage analysis from the haplotype data were conducted using GENEHUNTER.[8]

Sequence analysis. Mutation analysis of LAMP-2 was performed in two affected patients (IV-1 and IV-2) using an ABI PRISM 3100 automated sequencer (PE Applied Biosystems), as described.[2]

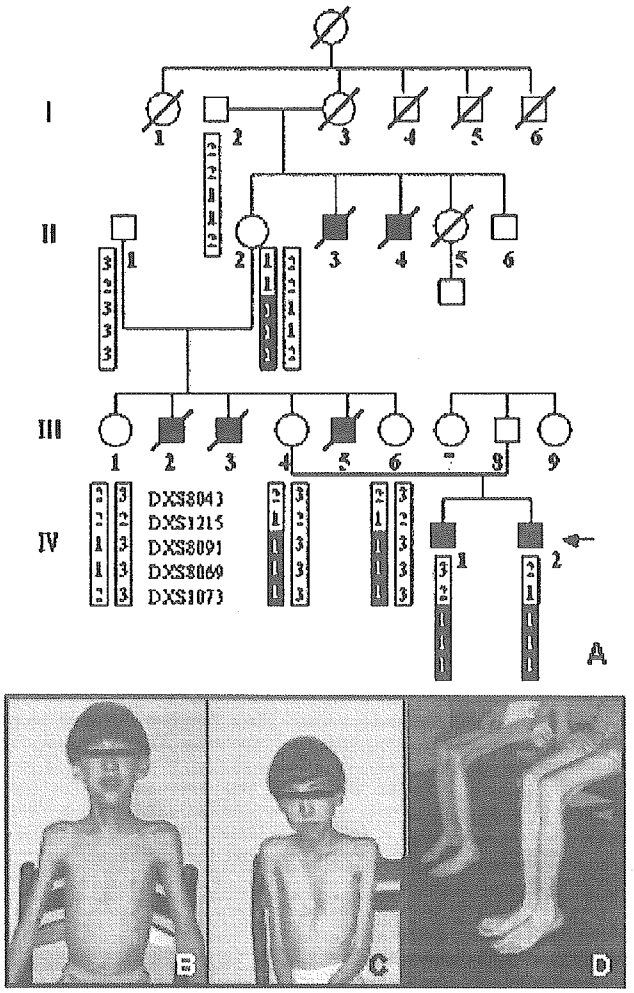

Figure 1. In the pedigree of the family (A), shaded boxes are the affected members. Symbols with diagonal lines represent deceased individuals. In the haplotype chart of this family, only informative regions (Xq27.2 to Xqter) are presented. The most important candidate region containing a common haplotype in three generations is highlighted by shaded boxes. Patient IV-2 (B and D) and Patient IV-1 (C and D) showed facial and neck muscle involvement, thoracic cage deformity, and severe generalized muscle atrophy.

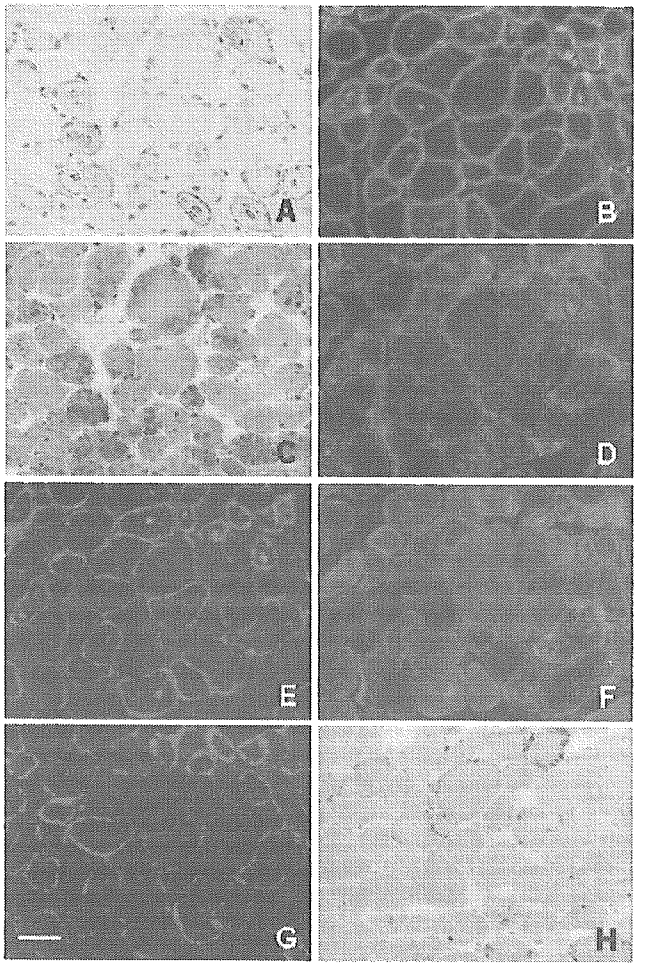

Figure 2. Muscle pathologic features (Patient IV-2). The vacuolar membranes have increased acetylcholinesterase (AChE) activities (A), and dystrophin is expressed in most intrasarcoplasmic vacuolar membranes (B). Strong acid phosphatase activity is observed inside vacuoles (C). Increased immunoreactivity of LAMP-2 is seen both at the surface membranes and within the cytoplasm of affected fibers (D). LIMP-1/CD63 is strongly stained at the sarcolemma and within the cytoplasm (E), and some cytoplasmic granular staining is colocalized with LC3 (F). Marked C5-9 membrane attack complex deposition is seen at the sarcolemma of almost all muscle fibers (G). By alizarin red, calcium deposition is seen at the sarcolemma and occasionally within the cytoplasm (H). Bar = 30 μm.

Histochemical and immunohistochemical analyses and electron microscopic studies. Serial frozen sections were stained with a battery of histochemical methods including hematoxylin and eosin (H-E), modified Gomori-trichrome, acid phosphatase, AChE, nonspecific esterase (NSE), periodic acid–Schiff, and alizarin red.

Immunohistochemical analysis was done using antibodies for LAMP-2 (H4B4; Developmental Studies Hybridoma Bank [DSHB]), LIMP-1/CD63 (H5C6; DSHB), dystrophin (NCL-DYS1; Novocastra Laboratories), C5b-9 membrane attack complex (MAC; DAKO Co.), microtubule-associated protein 1 light chain (LC3; kindly provided by Dr. Ueno[9]), CD59 (Biogenesis, Ltd.), dystrophin (NCL-DYS2; Novocastra), dysferlin (NCL-Hamlet 2; Novocastra), alpha sarcoglycan (Novocastra), caveolin-3 (Transduction Laboratories), and merosin (Chemicon International).

Electron microscopy was performed using a Hitachi H-7100 electron microscope.

Results. The skeletal muscle from patient IV-2 showed marked variation in fiber size with endomysial fibrosis. There are many intracytoplasmic vacuoles with activity for NSE (data not shown) and AChE (figure 2, A). Positive immunoreaction was observed at the vacuolar membranes with all five antibodies for sarcolemmal and extracellular matrix protein including dystrophin (figure 2, B). Within vacuoles, strong acid phosphatase activity was seen (figure 2, C), and vacuolar membranes showed LAMP-2 staining (figure 2, D), indicating the lysosomal nature of the vacuoles. Strong immunoreaction to LIMP-1/CD63, a lysosomal membrane protein, was observed both at the sarcolemma and inside the vacuoles (figure 2, E). LC3, having a crucial role for autophagosome formation,[9] was abundant in the cytoplasm, and some colocalized with LIMP-1/CD63 (figure

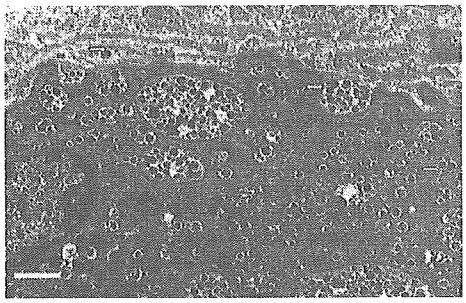

Figure 3. Electron microscopy shows large accumulation of dense globes and amorphous granules surrounded by a single layer membrane under sarcolemma or between the multiple layered basal lamina (white arrows). Some of these dense globes are encircled by a double-layered membrane (arrows). Some vacuoles are attached to the sarcolemma indicating exocytotic process. Bar = 1 μm.

2, F). MAC (figure 2, G) and calcium (figure 2, H) were markedly deposited at the sarcolemma in most fibers. CD59, an inhibitor of MAC, was positive in all muscle fibers, including MAC-positive ones (data not shown). Muscles from patients with Danon disease did not stain for LAMP-2. Membrane staining of LIMP-1/CD63 was weak, and MAC deposition was rarely observed (data not shown).

Electron microscopy of the patients' muscles revealed that numerous electron dense granules accumulated in various sizes of intracytoplasmic vacuoles (figure 3). Some larger granules were surrounded by double-layered membrane. The severely affected muscle fibers were surrounded by multilayered basal lamina wherein dense granules were also observed.

Mapping of the disease in this family using polymorphic microsatellite markers spanning the entire X-chromosome showed the highest multipoint lod score peak of 0.46 between markers DXS8069 and DXS1073. Other X chromosome region showed negative lod score, except for the small regions around DXS1226 (maximum 0.14) and DXS458 (maximum 0.08), suggesting that the causative gene may be localized in Xq28 (distal to DXS1215) (figure 1, A).

No mutation in *LAMP-2* was identified in the two affected patients examined.

Discussion. XMEA is clinically characterized as slowly progressive or nonprogressive myopathy with AVSF. The onset of symptoms usually ranges between ages 5 and 10 years, presenting with difficulty in climbing stairs and running without loss of ambulation. Lifespan is not altered. In contrast, our patients have more severe clinical manifestations with infantile hypotonia, dyspnea, and dysphagia. Some of the relatives died in early infancy, probably because of the same disease. Nevertheless, the pathologic features of our patients—multilayered basal lamina and intense sarcolemmal deposition of MAC and calcium in addition to AVSF—have been described as pathognomonic of XMEA.[6,10] In fact, the disease is pathologically indistinguishable from XMEA, suggesting allelism to XMEA. This notion is supported by the facts that the disease is transmitted through an X-linked recessive inheritance pattern and that haplotype analysis suggested Xq28, the chromosomal region for XMEA,[7] as a possible locus of this disease. The low lod score is due to small family size. Furthermore, similar pathologic findings were also reported in infantile AVM,[4] suggesting that it may also be allelic to XMEA. The identification of the XMEA gene will resolve the issue of allelism of these disorders to XMEA.

Although the genetic cause is still unknown, colocalization of LC3 and LIMP-1/CD63 in the patients' muscles, together with numerous dense granules on electron microscopy, suggests abnormal protein degradation as part of the pathomechanism in infantile AVSF as well as in XMEA.

Acknowledgment

The authors thank the patients and their families for their cooperation, Dr. Takashi Ueno (Jutendo University, Tokyo, Japan) for providing the LC3 antibody, Dr. Michio Hirano (Columbia University, New York, NY) for reviewing the manuscript, Dr. Jun Kimura (University of Iowa, Iowa City, IA) for comments on EMG findings, and Dr. Mina Astejada (National Center of Neurology and Psychiatry, Kodaira, Tokyo, Japan) for comments on the manuscript.

References

1. Sugie K, Noguchi S, Kozuka Y, et al. Autophagic vacuoles with sarcolemmal features delineate Danon disease and related myopathies. J Neuropathol Exp Neurol 2005;64:513–522.
2. Nishino I, Fu J, Tanji K, et al. Primary LAMP-2 deficiency causes X-linked vacuolar cardiomyopathy and myopathy (Danon disease). Nature 2000;406:906–910.
3. Saviranta P, Lindlof M, Lehesjoki AE, et al. Linkage studies in a new X-linked myopathy, suggesting exclusion of DMD locus and tentative assignment to distal Xq. Am J Hum Genet 1988;42:84–88.
4. Yamamoto A, Morisawa Y, Verloes A, et al. Infantile autophagic vacuolar myopathy is distinct from Danon disease. Neurology 2001;57:903–905.
5. Kaneda D, Sugie K, Yamamoto A, et al. A novel form of autophagic vacuolar myopathy with late-onset and multi-organ involvement. Neurology 2003;61:128–131.
6. Villanova M, Louboutin JP, Chateau D, et al. X-linked vacuolated myopathy: complement membrane attack complex on surface membrane injured muscle fibers. Ann Neurol 1995;37:637–645.
7. Minassian BA, Aiyar R, Alic S, et al. Narrowing in on the causative defect of an intriguing X-linked myopathy with excessive autophagy. Neurology 2002;59:596–601.
8. Kruglyak L, Daly MJ, Reeve-Daly MP, Lander ES. Parametric and nonparametric linkage analysis: a unified multipoint approach. Am J Hum Genet 1996;58:1347–1363.
9. Anasuma K, Tanida I, Shirato I, et al. MAP-LC3, a promising autophagosomal marker, is processed during the differentiation and recovery of podocytes from PAN nephrosis. FASEB J 2003;17:1165–1167.
10. Louboutin JP, Villanova M, Lucas-Heron B, Fardeau M. X-linked vacuolated myopathy: membrane attack complex deposition on muscle fiber membranes with calcium accumulation on sarcolemma. Ann Neurol 1997;41:117–120.

J Neuropathol Exp Neurol

Vol. 64, No. 6
June 2005
pp. 513–522

ORIGINAL ARTICLE

Autophagic Vacuoles with Sarcolemmal Features Delineate Danon Disease and Related Myopathies

Kazuma Sugie, MD, PhD, Satoru Noguchi, PhD, Yoshimichi Kozuka, PhD, Eri Arikawa-Hirasawa, MD, PhD, Mikihito Tanaka, PhD, Chuanzhu Yan, MD, Paul Saftig, PhD, Kurt von Figura, PhD, Michio Hirano, MD, Satoshi Ueno, MD, PhD, Ikuya Nonaka, MD, PhD, and Ichizo Nishino, MD, PhD

Abstract

Among the autophagic vacuolar myopathies (AVMs), a subgroup is characterized pathologically by unusual autophagic vacuoles with sarcolemmal features (AVSF) and includes Danon disease and X-linked myopathy with excessive autophagy. The diagnostic importance and detailed morphologic features of AVSF in different AVMs have not been well established, and the mechanism of AVSF formation is not known. To address these issues, we have performed detailed histologic studies of myopathies with AVSF and other AVMs. In Danon disease and related AVMs, at the light microscopic level, autophagic vacuoles appeared to be accumulations of lysosomes, which, by electron microscopy consisted of clusters of autophagic vacuoles, indicative of autolysosomes. Some autolysosomes were surrounded by membranes with sarcolemmal proteins, acetylcholinesterase activity, and basal lamina. In Danon disease, the number of fibers with AVSF increased linearly with age while the number with autolysosomal accumulations decreased slightly, suggesting that AVSF are produced secondarily in response to autolysosomes. Most of the AVSF form enclosed spaces, indicating that the vacuolar membranes may be formed in situ rather than through sarcolemmal indentation. This unique intracytoplasmic membrane structure was not found in other AVMs. In conclusion, AVSF with acetylcholinesterase activity are autolysosomes surrounded by secondarily generated intracytoplasmic sarcolemma-like structure and delineates a subgroup of AVMs.

Key Words: Autophagic vacuole, Autophagy, Danon disease, LAMP-2, Lysosome.

From the Departments of Neuromuscular Research (KS, SN, MT, CY, I Nishino) and Ultrastructural Research (YK), National Institute of Neuroscience, National Hospital for Mental (I Nonaka, I Nishino), Nervous and Muscular Disorders, National Center of Neurology and Psychiatry, Kodaira, Tokyo, Japan; the Department of Neurology (KS, SU), Nara Medical University, Kashihara, Nara, Japan; the Department of Neurology (EA-H), Juntendo University School of Medicine, Tokyo, Japan; the Department of Biochemistry (PS), University of Kiel, Kiel, Germany; Zentrum Biochemie und Molecular Zellbiologie (PS, KvF), Abteilung Biochemie II, Universität Göttingen, Göttingen, Germany; and the Department of Neurology (MH), Columbia University, New York, New York.

Send correspondence and reprint requests to: Ichizo Nishino, MD, PhD, Department of Neuromuscular Research, National Institute of Neuroscience, National Center of Neurology and Psychiatry (NCNP), 4-1-1 Ogawahigashi-cho, Kodaira, Tokyo 187-8502, Japan; E-mail: nishino@ncnp.go.jp

INTRODUCTION

Danon disease, an X-linked vacuolar cardiomyopathy and myopathy, is caused by primary deficiency of lysosome-associated membrane protein-2 (LAMP-2), a major lysosomal membrane protein (1–4). Muscle biopsies contain small autophagic vacuoles with cytoplasmic debris. The membranes of these vacuoles have structural features of sarcolemma and biochemical activities of acetylcholinesterase (AChE) and nonspecific esterase (NSE) (5). Although some sarcolemmal proteins, including dystrophin, have been detected in vacuolar membranes (3), the presence of other sarcolemmal proteins has not been studied. In addition, the pathomechanism by which LAMP-2 deficiency leads to the formation of these peculiar autophagic vacuoles with sarcolemmal features (AVSFs) is still unknown.

AVSFs are also seen in X-linked myopathy with excessive autophagy (XMEA) (6), infantile autophagic vacuolar myopathy (AVM) (7), and adult-onset AVM with multiorgan involvement (8). XMEA is clinically characterized by a mild pure skeletal myopathy. In contrast, infantile AVM involves both cardiac and skeletal muscles and patients die within several months after birth, whereas adult-onset AVM affects multiple organs including liver, kidney, and skeletal muscles. All of these diseases show multilayered basal lamina and the deposition of C5b-9 over the surface of the muscle fiber; these features are not seen in Danon disease. Nevertheless, these diseases are likely to share a common pathomechanism since they also have AVSF similar to those seen in Danon disease (9).

To delineate subtypes of AVMs and to gain insights into their pathomechanisms, we have performed detailed histologic evaluations of muscle from patients with Danon disease, XMEA, infantile AVM, and adult-onset AVM, and from LAMP-2 deficient mice (10, 11). Moreover, to evaluate the specificity of the AVSF we have also characterized autophagic vacuoles in other lysosomal myopathies, including acid maltase deficiency (AMD), sporadic inclusion body myositis (SIBM), and distal myopathy with rimmed vacuoles (DMRV), which has recently been shown to be the same disease as hereditary inclusion body myopathy (HIBM).

MATERIALS AND METHODS

Patients

We examined skeletal muscles of ten affected men from 8 families with genetically confirmed Danon disease. We also

confirmed this diagnosis by immunohistochemistry to demonstrate absence of LAMP-2 in skeletal muscle. Age at muscle biopsy varied from one year to 29 years, average 15 years ± 9. One patient underwent 2 biopsies from his left biceps brachii muscle at ages one year and from his right quadriceps femoris muscle at age 16 years (12). We also studied muscle from a 2-month-old boy with infantile AVM (7), a 41-year-old man with adult-onset AVM with multiorgan involvement (8), and an 18-year-old man with probable XMEA who showed typical clinicopathologic features of the disease but without a family history of myopathy.

Control specimens were obtained from 10 individuals with morphologically normal muscle. In addition, we also studied muscle from 21 patients with AMD (9 infants, 6 children, and 6 adults), 18 patients with DMRV/HIBM, and 20 patients with SIBM. We confirmed that all DMRV/HIBM patients had mutations in the gene encoding UDP-N-acetylglucosamine 2-epimerase/N-acetylmannosamine kinase (13).

Histochemistry

All biopsy specimens were taken from either the biceps brachii or quadriceps femoris muscle. These tissue samples were frozen in liquid nitrogen-cooled isopentane for histochemistry and immunohistochemistry. Transverse serial frozen sections of 8-μm thickness were stained with hematoxylin and eosin (H&E), modified Gomori trichrome, and a battery of histochemical methods, including AChE and NSE stains.

Immunohistochemistry

We performed indirect immunofluorescence staining on 5-μm serial cryosections of muscle according to previously described methods (14). These sections were incubated at 37°C for 2 hours with primary mouse monoclonal IgG antibodies against AChE, lysosomal membranous proteins: LAMP-1, lysosomal integral membrane protein-1 (LIMP-1), LIMP-2, and 19 primary monoclonal or polyclonal antibodies against various sarcolemmal proteins and extracellular matrix proteins (Tables 1 and 2). We also used antibodies against an intralysosomal protein, cathepsin L, and endosomal proteins, VAMP-7, Rab5, transferrin receptor (TfR), and low-density lipoprotein receptor (LDL-R). These were subsequently incubated at room temperature for 1 hour with a secondary antibody, fluorescein isothiocyanate (FITC)-labeled goat F(ab')2 anti-mouse IgG (Leinco Technology, St. Louis, MO) or anti-rabbit IgG (H&L) (Leinco). For double immunolabeling using mouse monoclonal anti-LIMP-1 and rabbit polyclonal anti-dystrophin antibodies (a generous gift from Dr. Imamura), we used two secondary antibodies: FITC-labeled anti-mouse IgG (Leinco) and rhodamine-labeled anti-rabbit IgG (Leinco). We also have stained serial sections with Alexa 488 conjugated α-bungarotoxin (Molecular Probe, Eugene, OR) and were examined by fluorescence microscopy. Furthermore, in other sections, after incubation with primary antibodies we stained with the avidin-biotin-peroxidase complex method (Vector Laboratories, Burlingame, CA) using another secondary antibody: biotinylated goat anti-mouse IgG (Vector). The reaction was visualized with 3,3'-diaminobenzidine (DAB) as the substrate, yielding a brown reaction product. Normal mouse IgG, diluted to the same concentration as the primary antibodies, was used as a negative control.

To estimate presence of the sarcolemmal proteins in vacuolar membrane, we scored the signal of the antibodies from negative (−) to strong (+++) relative to their immunoreactivity in the sarcolemma. The strong score (+++) indicates that the reactivity level in vacuoles equals that in the sarcolemma. Moreover, we counted the numbers of 1) muscle fibers with intracytoplasmic vacuoles highlighted with dystrophin, and 2) muscle fibers with intracytoplasmic overexpression of LIMP-1, in randomly selected fields of all the patients, and calculated the average percentages of both types of muscle fibers in each patient. Statistical analysis of the correlation between the age of the patients and the numbers of muscle fibers immunoreacting dystrophin or LIMP-1 was performed using linear regression.

Electron Microscopy

For electron microscopy, biopsy specimens were fixed in buffered 2% isotonic glutaraldehyde at pH 7.4, postfixed in osmium tetroxide, and embedded in Epoxy resin. Ultrathin sections were stained with uranyl acetate and lead nitrate, and examined with an H-7000 electron microscope (Hitachi, Tokyo, Japan).

Immunoelectron Microscopy

We performed immunoelectron microscopy by preembedding labeling methods. We used muscle biopsy specimens frozen in liquid nitrogen-cooled isopentane without paraformaldehyde prefixation. The specimens were cut in a cryostat into 10-μm transverse sections without thawing and fixed in chilled 4% paraformaldehyde solution in 0.1M phosphate buffer (pH 7.4) for 10 minutes. The fixed sections were washed 5 times in phosphate-buffered saline (PBS). To eliminate nonspecific reactions, sections were incubated for 30 minutes at room temperature in PBS containing 10% normal goat serum and 1% bovine serum albumin (BSA) with PBS. The sections were then incubated at 4°C overnight with one of the following primary mouse monoclonal IgG antibodies: LIMP-1 and the C-terminus of dystrophin. After washing for 30 minutes in PBS, the sections were incubated at 4°C overnight with a secondary antibody: 10-nm-gold-labeled rat anti-mouse antibody (British Biocell International, Cardiff, UK). Subsequently, the sections were fixed in 0.5% glutaraldehyde and postfixed in osmium, and embedded in Epoxy resin. Ultrathin sections were counterstained with uranyl acetate and lead nitrate.

LAMP-2-Deficient Mice and Pathological Methods

We analyzed tibialis anterior muscle from 2 LAMP-2-deficient mice (10, 11) at ages 4 months and 16 months and age-matched normal mice. Muscle specimens were frozen in liquid nitrogen-cooled isopentane for histochemistry and immunohistochemistry or fixed with glutaraldehyde for electron microscopy. Transverse serial frozen sections of 10-μm thickness were stained with H&E, modified Gomori trichrome,

TABLE 1. Summary of Histochemistry and Immunohistochemistry in Various Myopathies with Autophagic Vacuoles

			Expression on Vacuolar Membrane		
	Manufacturer of Antibody	Dilution	Danon Disease and Related AVMs	Rimmed Vacuolar Myopathies	AMD
Histochemistry					
NSE	–	–	+++	–	–
AChE	–	–	+++	–	–
PAS	–	–	+	–	+++
Acid P	–	–	± to ++	++	++
Immunohistochemistry					
AChE	Chemicon, Temecula, CA	1:2000	+++	–	–
AChR	Molecular Probe, Eugene, OR	1:300	–	–	–
C-terminus of Dystrophin	Novocastra, Newcastle Upon Tyne, UK	1:100	+++	– to +	– to +
Rod domain of Dystrophin	Novocastra	1:50	+++	– to +	– to +
N-terminus of Dystrophin	Novocastra	1:20	+++	– to +	– to +
α-Sarcoglycan	Novocastra	1:100	+++	– to +	– to +
β-Sarcoglycan	Novocastra	1:100	+++	– to +	– to +
γ-Sarcoglycan	Novocastra	1:200	++	– to +	– to +
δ-Sarcoglycan	Novocastra	1:50	+++	– to +	– to +
α-Dystroglycan	Upstate, Lake Placid, NY	1:100	++	– to +	– to +
β-Dystroglycan	Novocastra	1:200	+++	– to +	– to +
Dystrobrevin	RDI, Flanders, NJ	1:100	++	– to +	– to +
Dysferlin	Novocastra	1:50	++	– to +	– to ±
Utrophin	Novocastra	1:50	+	– to ±	–
Caveolin-3	Transduction Labs, Lexington, KY	1:100	++	– to +	– to +
β-Spectrin	Novocastra	1:100	++	– to +	– to +
Laminin α2	Chemicon,	1:5000	++	– to +	– to +
Integrin β1	Genex, Helsinki, Finland	1:100	+++	– to +	– to +
Perlecan	Chemicon	1:100	++	– to +	– to +
Agrin	A generous gift from Dr. Sugiyama (32)	1:100	++	– to +	– to +
Fibronectin	Biomedical Tech., Stoughton, MA	1:1000	++	– to ±	– to ±
Collagen IV	Novocastra	1:1000	– to +	– to ±	– to ±
Collagen VI	ICN, Aurora, OH	1:500	– to +	–	– to ±

Both antibodies against fibronectin and agrin were rabbit polyclonal antibodies. All the other antibodies were mouse monoclonal antibodies. AChR was evaluated by binding to α-bungarotoxin. AMD, acid maltase deficiency; NSE, non-specific esterase; AChE, acetylcholinesterase; PAS, periodic acid Schiff; Acid P, acid phosphatase; AchR, acetylcholine receptor.

and a battery of histochemical methods, and the same immunohistochemical methods described above.

RESULTS

Histochemistry and Immunohistochemistry

By routine histologic studies, the vacuolar membranes in Danon disease, probable XMEA, infantile AVM and adult-onset AVM were essentially identical (Table 1). All muscle samples showed mild to moderate variation in fiber size. There were no necrotic fibers except in muscle from adult-onset AVM, which revealed a few necrotic and regenerating fibers. There were scattered small basophilic granules rather than vacuoles in the muscle fibers in H&E-stained sections (Fig. 1). Histochemistry revealed AChE and NSE activities in the vacuolar membranes and the vacuolar structures of the granules. Immunohistochemistry also confirmed presence of AChE in those vacuoles. However, they did not bind to α-bungarotoxin, indicating the absence of acetylcholine receptors (AChRs) in the vacuolar membranes.

By immunohistochemistry, the AVSF reacted for all the tested sarcolemmal and extracellular matrix proteins in the vacuolar membranes in muscle from patients with Danon disease and related AVMs, although reactivity levels of the proteins were variable (Table 1; Fig. 1). However, only collagens IV and VI showed less intense reactivity in the vacuolar membranes than that in the sarcolemma. Most of the AVSFs were scattered throughout the cytoplasm rather than clustered in the subsarcolemmal region. On serial transverse 5-μm sections, most of the AVSFs formed a closed space and the vacuolar membranes were not connected to the sarcolemma with only a few exceptions (Fig. 1Y). Longitudinal sections demonstrated the oval shape of the AVSF, confirming the closed structure of the vacuoles (Fig. 1Z). Vacuolar membranes connected to the sarcolemma were seen in only 2 patients; both were more than 20 years old.

In muscle from patients with Danon disease, LIMP-1, a lysosomal membrane protein, showed accumulations scattered

TABLE 2. Summary of Lysosomal and Endosomal Proteins for Immunohistochemistry in Danon Disease and Related AVMs

Antigen	Manufacturer	Dilution	Expression in the Muscle Fibers
Lysosomal protein			
LAMP-1	Developmental Studies Hybridoma Bank (DSHB), Iowa City, IA	1:100	++
LAMP-2	DSHB	1:100	–
LIMP-1	DSHB	1:100	+++
LIMP-2	A generous gift from Dr. Tanaka (10)	1:200	+
Cathepsin L	Abcam, Cambridge, UK	1:100	+
Endosomal protein			
Rab5	BD Bioscience, Franklin Lakes, NJ	1:50	+
LDL-R	Progen Biotechnik, Heidelberg, Germany	1:100	+
VAMP-7	A generous gift from Dr. Galli (29)	1:200	++
Transferrin R	Lab Vision, Fremont, CA	1:100	+

Antibody against LIMP-2 was rabbit polyclonal and antibody against LDL-R was chicken polyclonal. All the other antibodies were mouse monoclonal.

throughout the fibers in a distribution identical to that of the small basophilic granules on H&E-stained sections (Fig. 2; Table 2), indicating that most autophagic vacuoles in Danon disease are autolysosomes. These autolysosomal accumulations were surrounded by dystrophin-positive membranes in some fibers but not in others (Fig. 2). LAMP-1 and LIMP-2 showed slightly increased expression in fibers with LIMP-1-positive granules (data not shown). Muscle fibers with dystrophin-positive vacuoles accounted for 0.5% to 14.3%, increasing in proportion with age ($y = 0.016 + 0.40x$, $r = 0.94$; Fig. 3). Muscle fibers with autolysosomal accumulations, both with and without dystrophin-positive vacuolar membranes, accounted for 23.7% to 28.7%, showing a slight tendency to decrease with age ($y = 28.6 - 0.15x$, $r = 0.71$; Fig. 3).

LDL-R, TfR, and Rab5 showed mild upregulation mainly in fibers with autolysosomal accumulations in Danon disease and related AVMs (Table 2). Cathepsin L was expressed weakly, mainly in fibers with autolysosomal accumulations. Only VAMP-7 was strongly expressed, mainly in the non-vacuolated fibers without autolysosomal accumulations.

There were occasional intracytoplasmic vacuoles with sarcolemmal proteins in muscles from patients with other AVMs (i.e. DMRV/HIBM, SIBM, and AMD) but their presence was less consistent than in Danon disease and related AVMs. In addition, they never showed AChE or NSE activity. In DMRV/HIBM and SIBM, fibers with sarcolemmal protein-associated vacuoles accounted for approximately 5% to 15% of fibers with rimmed vacuoles (Fig. 4; Table 1). In AMD, sarcolemmal and extracellular matrix proteins were present in some vacuolar membranes. The frequency of fibers with sarcolemmal proteins-associated vacuoles was less than 5% of vacuolated fibers in infantile AMD, and 10% to 15% of vacuolated fibers in childhood and adult-onset AMD.

Electron Microscopy and Immunoelectron Microscopy

In Danon disease and related AVMs, electron microscopy revealed scattered clusters of autophagic vacuoles containing cytoplasmic debris, electron dense materials, and myeloid bodies. Some of these autophagic vacuoles had basal lamina on the luminal side, while other clusters were not limited by a membrane (Fig. 5).

Immunoelectron microscopy showed many autophagic vacuoles; however technical limitations posed by preparing samples from frozen tissue without prefixation prevented us from clearly defining vacuolar membranes. At higher magnification, dystrophin signals were detected on the cytoplasmic side of the vacuolar membrane and along the periphery of the vacuoles (Fig. 5). In contrast, the LIMP-1 antibody signals were associated with autophagic materials including glycogen particles and cytoplasmic debris within the vacuoles, suggesting that the vacuoles are limited by membranes with sarcolemmal features and contain multiple small autophagic vacuoles derived from autolysosomes.

Muscle Pathology in Mice

Muscles from LAMP-2-deficient mice at both 4 and 18 months of age showed features of AVSFs at both light and electron microscopic levels. There were slight variations in fiber size and small vacuoles with basophilic granules by H&E. The granules contained acid phosphatase-positive material. These AVSFs had AChE and NSE activities similarly to those in Danon disease. The frequency of muscle fibers with the AVSFs decorated by NSE and AChE activities was 0.4% at 4 months and 8% at 16 months (data not shown). On immunohistochemistry, the vacuolar membranes were stained with antibodies against dystrophin and other sarcolemmal proteins as well as extracellular matrix proteins, whereas LAMP-2 was completely absent in the muscle. On electron microscopy, there were scattered intracytoplasmic autophagic vacuoles with glycogen particles and cytoplasmic debris (data not shown).

DISCUSSION

In muscle from patients with Danon disease and related AVMs, the membranes of AVSF showed immunoreactivity for all of the sarcolemmal and extracellular matrix proteins tested. Dystrophin and dystrobrevin are cytoskeletal proteins localized along the cytoplasmic side of the sarcolemma (15). Sarcoglycans and β-dystroglycan are transmembranous proteins and are components of "dystrophin bolts" (16). Utrophin